Study of Cholesterol in Tethered Membrane Using Coarse-Grained Molecular Dynamics Simulations

by

Yan Duan

B.Sc in Engineering Physics, The University of Alberta, 2014

A THESIS SUBMITTED IN PARTIAL FULFILLMENT OF
THE REQUIREMENTS FOR THE DEGREE OF

MASTER OF APPLIED SCIENCE

in

The Faculty of Graduate and Postdoctoral Studies

(Electrical and Computer Engineering)

THE UNIVERSITY OF BRITISH COLUMBIA

(Vancouver)

September 2015

Abstract

This thesis presents a study of cholesterol's effects on archaebacterial cell membranes using coarse grain molecular dynamic simulations. As a major component in biological membranes, cholesterol is closely related to the dynamics of lipids and biomechanical properties of the membrane. A coarse grained molecular dynamics (CGMD) model is constructed to study the membrane properties. The CMGD model provides insights into the diffusion dynamics of lipids, membrane thickness, line tension, and surface tension corresponding to different cholesterol levels. The CGMD simulation results are validated using experimental measurements from a tethered archaebacterial bilayer lipid membrane. The membrane is tethered onto an inert gold bioelctronic interface, which allows the experimental measurements to be performed using standard laboratory equipments. A fractional order macroscopic model is introduced to link microscopic simulation results with macroscopic experimental measurements. To ensure the bioelectronic interface does not affect the membrane dynamics and biomechanics, it is shown that variations in the position dependent water density are negligible near the surface of the membrane. Furthermore, the Percus-Yevick equation is used to confirm that harsh repulsive forces play a negligible role in the long range dynamics of the water density profile.

Preface

This thesis consists of three main chapters. The first chapter gives the motivation of the thesis and five levels of abstraction for cell membrane modeling. The second chapter provides a comprehensive introduction on necessary concepts and theories to understand molecular dynamics, and its simulation schemes and tools. The third chapter is largely based on work conducted in statistical signal processing lab at University of British Columbia, by Dr.William Hoiles, Prof.Vikram Krishnamurthy and Yan Duan. I was responsible for all the coarse-grained simulation, derivation and application of Percus-Yevick equation for the water density profile, numerical solution of Volterra differential-integral equation, and parameter estimations for the fractional order macroscopic model.

Table of Contents

List of Tables

List of Figures

Acknowledgements

I would like to first thank my supervisor Prof.Vikram Krishnamurthy at UBC. Not only he offers me valuable directions and support for my graduate study, but also his great passion and insights on science and engineering encourage me to make more contributions to our community.

I am truly honored to work with Dr.William Hoiles, as a beginner in this field, I got valuable training from him. His keen insights, comprehensive knowledge and kind patience showed me the characteristics that an excellent scholar would possess.

I am very grateful for my family members. Their encouragements and loving supports are so important, that I could have been a totally different person without them.

Finally I would like to express my appreciation to my dear friends and colleagues, it's always good time to talk to them and learn from them.

Dedication

To my family: Shaoan, Defang, Bing, my cousins and my grandparents.

Chapter 1

Introduction

1.1 Motivation: the Biosensor

In 1956, Dr.Leland C. Clark conducted his famous experiment on oxygen detection using platinum, where he placed the enzyme Glucose Oxidase (GOD) close to the surface of platinum, thus to trap oxygen against the electrodes using a piece of dialysis membrane [13]. It was the first time that element recognition was achieved by using bio-materials. Since then, substantial research has emerged to investigate the element recognition process involving bio-materials, which has further led to the developments of biological sensors, or the simply-called "biosensors".

Commercialized biosensors are already in use in areas such as healthcare monitoring, industrial processing and environmental pollution control [50]. Even though this is the case, further improvements on biosensors to achieve higher sensitivity of element detection, wider scope of applications, and lower production costs for biosensors are strongly demanded by markets [51]. This necessitates a thorough understanding of element recognition process involved in biosensors.

A standard biosensor consists of a recognition component called bioreceptor, and a corresponding transducer component. A bioreceptor interacts with the desired chemical analytes and the interaction is detected by the transducer. The transducer produces a measurable electrical signal, which is sent to an electronic system composed of an amplifier and a display circuit. The biosensor structure is summarized in Fig. 1.1. The class of bioreceptor includes a variety of biomolecules such as membrane proteins, enzymes, antibodies and nucleic acids. An electrochemical transducer is normally a metal electrode, while other types such as optical and thermal transducers are also in use [20]. More details on choices of transducers are introduced in Sec. 1.3.

Since many of the element recognition processes occur at the cell membrane, investigation of cell membrane properties has played an important role in biosensor research. Furthermore, due to the difficulty of using living animal cell membranes, artificial lipid membranes have become the main

source to obtain insights into the recognition processes occurring in the proximity of the cell membrane. In this thesis, a study on synthetic archaebacterial membrane will be presented.

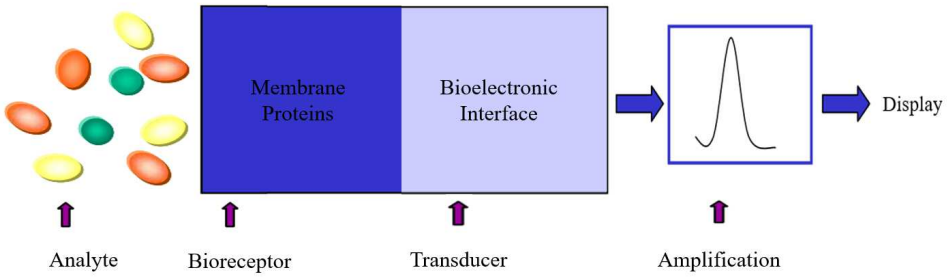

Figure 1.1: Overview of a biosensor, consisting of a bioreceptor (membrane proteins) and a transducer (metal electrode/bioelectronic interface), which are connected to an amplifier and a display circuit

1.2 Cell Membrane System

The cell membrane is composed of three primary components: membrane lipids, macromolecules, and the cytoskeletal filaments [44]. Fig. 1.2 summarizes the membrane structure.

Membrane lipids are a group of biological compounds that possess amphiphilic property, which means that each lipid molecule has one water-soluble end and one non-water-soluble end. The amphiphilic property forces lipid molecules to group together to form a double-layer structure in water environment, so a cell membrane is often referred as "lipid bilayer" in many contexts. Different components of membrane lipids have different effects on cell shape, permeability and organization of macromolecules [44]. Membrane lipids contain a wide variety of biological compounds, the most common ones include phospholipids and sterols such as cholesterol. For artificial membranes, various synthetic phospholipid derivatives can be used [16]. In this work, a synthetic archaebacterial membrane composed of zwittrionic C20 diphytanylether-glycero-phosphatidylcholine lipid (DphPC) and C20 diphytanyl-diglyceride ether lipid (GDPE) is investigated.

Macromolecules refer to a group of large (more than 1000 atoms) molecules including nucleic acids, carbonhydrates and proteins. In the case of cell membrane, macromolecules usually refer to proteins. The membrane pro-

teins can be classified into two functional classes: transport protein and membrane receptor [44]. As one type of bioreceptors, membrane receptor proteins transmit electrical signals between intracecullar and extracellular environments. Transport proteins, on the other hand, aid in transmembrane movements of ions and large molecules by forming channels/-pores. Furthermore, cytoskeletal filaments provide the physical structural support for the membrane.

This thesis studies the properties of lipids, such as diffusion dynamics, membrane thickness and surface/line tension. Therefore, a simple membrane model (archaebacterial membrane) that only includes membrane lipids is constructed.

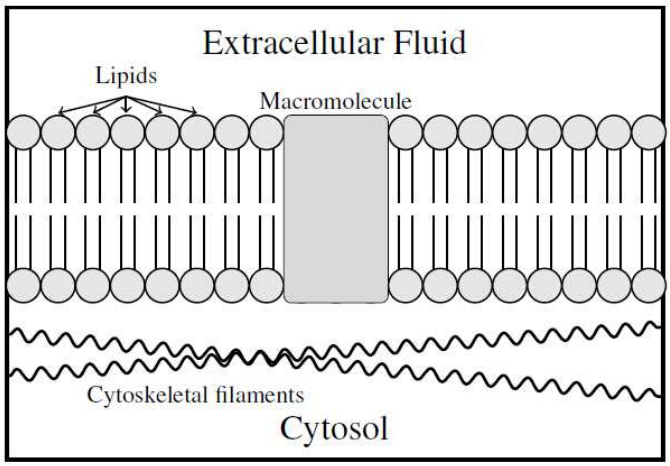

Figure 1.2: Schematic of a natural biological membrane. The extracellular fluid represents the contents outside the cell, and the cytosol is the interior of the cell with the membrane separating the two domains. Note that biological membranes are composed of thousands of different components (macromolecules, lipids, chemical species)

1.3 Bioelectronic Interface

Electrical instrumentation is required to measure the electrical signals generated from artificial membrane. Thus to perform measurements for a biosensor, we need to introduce a transducer, that is, a bioelectronic interface to connect the biological system to the electrical instrumentation.

We consider a tethered membrane system connected to a bioelectronic

interface, which is the standard set up for an electrochemical biosensor. A particularly useful bioelectronic interface comprises of inert gold electrodes. They have advantages over redox active electrodes such as biopolymers, because redox active electrodes will tend to force the tethers to dissociate from the electrode surface, thus to destroy the membrane. Also, redox active electrodes will release metal ions into solution, which can interfere with the electrophysiological response of proteins and peptides [14]. The inert gold electrode, however, capacitively couples the electronic domain to the physiological domain without the issues associated with redox electrodes.

However, with the presence of gold interface, the so-called "diffusion limited effect" need to be considered in modeling of tethered membrane system. The diffusion limited effect refers to the fact that a fast reaction will be triggered if membrane components diffuse and contact the gold surface, such effect at the interface can cause the charge transfer of bio-molecules, which are highly undesirable [53]. The problem of diffusion limited effect, and its solution will be discussed with more details in Sec. 3.6 of this thesis.

1.4 Abstractions in Bio-System Modeling

As mentioned above, a bioelectronic interface should connect the tethered membrane system and electric instrumentation. However, the problem is, how to make interpretations of electrical measurements thus to explain membrane characteristics? The investigation on membrane system is to study microscopic properties such as diffusion dynamics and membrane thickness, but the data that can be measured is macroscopic, such as voltage and current. Thus a key to the development of novel membrane biosensor is an accurate mathematical model of the cell membrane, which is able to interpret the macroscopic measurements and reflects corresponding microscopic membrane properties correctly. Such a model must link the microscopic dynamics of water, lipids, peptides to experimental measurements at a macroscopic time and length scale.

There are five levels of modeling abstraction of mathematical models that have been used for modeling dynamics of cell membrane. For these abstractions, more the details considered for the system, more is the computational power and time required for the simulation, and vice versa. A schematic diagram for the five levels of abstraction for bio-systems is summarized in Fig. 1.3.

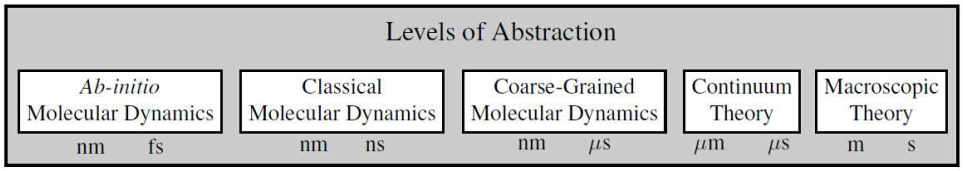

Figure 1.3: Schematic diagram illustrating the length and timescale achievable by the atomistic to macroscopic simulation methods

1.4.1 Ab-initio Molecular Dynamics

The "Ab-initio" molecular dynamics, or the "from the beginning" molecular dynamics model, is the model that takes into account the most comprehensive details for a system. Ab-initio includes both classical Newton's physics and quantum mechanical Schrodinger's equations for the dynamics of target system, which might include particles such as water, ions, membrane lipids, proteins, and peptides. This is the model that provides the most detailed description of a real system. However, due to these (sometimes unnecessarily) detailed equations, an excessive computational power is required. Thus Ab-initio molecular dynamics could only attain membrane length scale of nanometer and simulation time in an order of femtosecond, which is too small compared to the data that can be obtained from any experimental measurement [39]. Therefore such method is not quite popular in bio-system modeling so far.

1.4.2 Molecular Dynamics

Molecular dynamics (MD) is a simplification of the above "Ab-initio" molecular dynamics model. The quantum mechanical Schrodinger's equations considered in "Ab-initio" molecular dynamics are ignored in this model, that is, the matrix representation of semi-empirical potential from quantum mechanics is not used in MD, and only empirical potentials associated with chemical bonds, bond angles and non-bonded forces are considered into MD [42]. More details of molecular dynamics would be discussed in the next chapter. It's also worth noting that, although only Newtonian equations are evaluated for each time step of MD simulation, still merely a length order of nanometer and time order of nanosecond can be achieved by using MD.

1.4.3 Coarse-Grained Molecular Dynamics

Coarse-Grained Molecular Dynamics (CGMD) is a further simplification based on molecular dynamics. By grouping certain atoms together into coarse-grained beads, with the bead-to-bead interactions empirically parameterized, membrane dynamics can still be evaluated using Newton's equations of motion [47]. Such simplification allows CGMD simulations to achieve simulation time scale of microseconds with a system size of tens of nanometers, which are good enough to match most real membrane dynamics that can be measured by experiments. The main results presented in this thesis would be based on CGMD simulations.

1.4.4 Continuum Theory

Despite their different levels of abstraction, the above three molecular dynamics models are considering discrete particles of a system. Thus if the number of particles in target system is large, the efficiency of computation can be limited. Therefore, a more simplified class of models is to treat the discrete entities as continuous densities, which represent the space-time average of the microscopic motion of particles. The most well-known continuum model should be the Poisson-Nernst-Planck system of equations for diffusion process of ion transport, which combines the Poisson equation from electrostatics, and the Nernst-Planck equation for diffusion [60]. Such a significant simplification allows continuum models to achieve simulation time scale of the the order of microseconds, with a system size of micrometers.

1.4.5 Macroscopic Model

As its name suggests, a macroscopic model describes a bio-system system by using macroscopic parameters, which can be obtained from experimental measurements. Normally these parameters can be defined to be any entity, and there's even no specific physical interpretation required for them: as long as these estimated parameters can fit the experimental measurements, the macroscopic model can be regarded to be successful. In this thesis, a fractional macroscopic model is introduced to estimate biological parameters, such as tethered membrane conductance and capacitance based on experimental measurements. Due to the free choice of parameters for the macroscopic models, there is no limit to the attainable scales of length and time.

1.5 Thesis Contributions

This thesis is composed of four chapters, which include an introductory chapter for fundamental molecular dynamics, and a chapter on the study of cholesterol in tethered membrane using CGMD simulations.

Chapter 2 provides an introduction to the fundamental newtonian physics involved in molecular dynamics algorithms, along with common force fields (potential functions) including MARTINI force field used in CGMD simulations. Then a four-step MD simulation scheme is introduced along with the simulation engine GROMACS. Details on configuration of GROMACS files and programs are provided, with an introduction to common terminologies and algorithms used in MD simulations.

Chapter 3 presents the core research work in this thesis. The effects of cholesterol on tethered archaebacterial membrane system are studied by using Coarse-Grained molecular dynamics simulations. The archaebacterial membrane consists of 70% DphPc and 30% GDPE lipids, which are tethered onto a gold bioelectronic interface. By following the simulation scheme introduced in Chapter 2, the CGMD simulation based on MARTINI force field is used to study properties of membrane lipids, as cholesterol level varies from 0% to 50%.

The following results are presented regarding membrane properties affected by cholesterol:

- In order to match the simulation model with real membrane used in experiments, a CGMD model for a tethered archaebacterial membrane is introduced. The CGMD simulation protocol is provided following the four-step scheme introduced in Chapter 2.

- To make reliable measurements in experiments, it is crucial to figure out the region that is not affected by the bioelectronic interface, which can change the diffusion dynamics of membrane and water. Thus the position-dependent water density profile at the bioelectronic interface is studied. An analytical solution of Percus-Yevick equation is obtained, to show that the water density profile doesn't vary much as far as 4nm from the interface, and short-range interactions in Lennard-Jones potential contribute little to affect water density profile.

- Lipids undergo three regimes of diffusion: ballistic, subdifusion and Fickian diffusion, which are predicted by mode-coupling theory. Although the three diffusion dynamics can be obtained by Volterra integral-differential equation, however, due to the excessive computational pow-

er required by its numerical solution, CGMD simulation results are used to analyze diffusion dynamics of membrane instead. It is shown that cholesterol concentration does not affect the transition time between the subdiffusion and Fickian diffusion, and cholesterol concentration only affects the diffusion coefficient of lipids in Fickian diffusion regime. As cholesterol concentration increases, the lipid diffusion coefficients decrease.

- The effects that cholesterol have on biomechanics properties of membrane are also presented by using CGMD simulation results. It is shown that as the cholesterol concentration increases from 0% to 50%, the membrane thickness increases, the membrane line tension increases, while the membrane surface tension increases up to 30% cholesterol in membrane then decreases.

- To link the macroscopic experimental measurements with microscopic simulation results, and to account for the diffusion limited effects due to the bioelectronic interface presented in the tethered membrane system, a fractional order macroscopic model is introduced. The tethered membrane is modeled by a fractional order RC circuit, whose parameters are obtained by a least-square estimator.

Finally, Chapter 4 briefly summarizes the key results, and comments on the suggestions for future research related to the work presented in this thesis.

Chapter 2

Fundamental Molecular Dynamics

2.1 Basic Algorithm and Force Fields

Currently there are two classes of simulation techniques in computational chemistry and biology: molecular dynamics (MD) and Monte Carlo simulation [22]. Monte Carlo molecular modeling method starts from an initial microstate, then keeps moving to the desired state according to the desired ensemble's Boltzman probability distribution [22]. In compasiron, MD is a more universal technique, especially in non-equilibrium ensemble and analysis of dynamic scenarios. Ever since it was first proposed by Alder and Wainwright in the late 1950's [1] to study the interactions of hard spheres, MD has been used extensively for studying the structural and dynamical properties of molecules.

2.1.1 Global MD Algorithm

An MD algorithm starts by assigning initial positions and velocities to all particles within the system being considered. The algorithm looks for a global optimal value of energy potential function for the initial system. A step called "energy minimization" guarantees that the initial positions and velocities of all particles can be accepted (i.e states of atoms are within the range pre-defined by the simulation engine). Finally, for each time step, a set of classical Newtonian equations of motion is solved for i^{th} particle of a system, which includes N interacting particles [28]:

$$\begin{aligned} m_i \frac{\partial^2 r_i}{\partial t^2} &= F_i \\ \frac{dr_i}{dt} = v_i \quad & \frac{v_i}{dt} = \frac{dv_i}{dt} \end{aligned} \tag{2.1}$$

where m_i is the mass of the i^{th} particle, t the time, r_i the vector of particle relative to the origin, and F_i the interactive forces applied on the particle. The interactive forces are the derivatives of the potential function $E(r_1, r_2, ...r_N)$:

$$F_i = \frac{-\partial E}{\partial r_i} \tag{2.2}$$

where the potential function is given as a combination of bonded and non-bonded interactions between the particles. A potential function can be shown as follows:

$$\begin{aligned} E(r_1, ..., r_N) = & \sum_{bonds} k_a(l - l_0)^2 + \\ & \sum_{bonds} k_b(\theta - \theta_0)^2 + \\ & \sum_{torsion} k_c[1 + cos(n\omega - \gamma)] + \\ & \sum_{atompairs} 4\epsilon_{ij}[(\frac{\sigma_{ij}}{r_{ij}})^{12} - (\frac{\sigma_{ij}}{r_{ij}})^6] + \\ & \sum_{atompairs} k\frac{q_i q_j}{r_{ij}} \end{aligned} \tag{2.3}$$

The first and second term are the covalently bonding energies, which are induced by deformations of bond length l and bond angle θ, respectively; the third term describes the energy due to rotation around the chemical bond, the first three terms represent the bonded potential. The last two terms describe the non-bonded interactions between all atom pairs, which include Lennard-Jones potential and the Coulomb electrostatic potential, respectively. k_a, k_b, k_c are all constants related to specific atom interactions, ϵ is the permittivity constant and k is the Coulomb constant. r is the distance between atoms, while σ is the distance at which inter-atom potential is zero.

By solving the newtonian equations 2.1, the particle trajectories which are represented by coordinates $r_{i=1,2,...,N}$ can be obtained. Based on the initial conditions: potential interaction E, initial positions r and velocities v , with temperature and pressure configured to be desired values, the simulation keeps updating the coordinates of the atoms by solving Newtonian equations, thus the coordinates of particles are generated at specific time steps.

To summarize, a molecular dynamics simulation involves the following three steps:

1. Input initial conditions, which include pre-defined potential functions (force fields), initial positions and velocities of particles
2. Compute forces by solving equation 2.2
3. Update the system states (positions, velocities and energies of all particles) by solving equation 2.1

2.1.2 Force Fields

As described in equation 2.3, force field (or equivalently, potential function) can be fully described by bonded and non-bonded interactions. Before starting any molecular dynamics simulation, we need to pre-define the parameters that describe the potential function properly, thus to compute the forces and update the system trajectories. Different force fields are made and used for different purposes. The most comprehensive force field is the so-called "all-atom" force field–that is, all atoms are considered to be assigned interaction parameters [69]. However, limited by computational power and simulation time, mainstream force fields usually ignore some unimportant atoms such as non-polar hydrogens, which contribute insignificant interactions to a system. In this section, one common widely used force field is introduced, which will be used in the simulations in Chapter 3 of this thesis.

Coarse Grained Force Fields: MARTINI

The significance of molecular dynamics simulations is based on the fact that, mechanical and chemical processes at atomistic level are able to reflect real states of system at macroscopic level. Therefore, an MD simulation needs to match a real experiment at a reasonable scale of space and time. This means that, an ideal MD simulation should not only take into account maximum details for topology (nano-meter scale) of the target system, but also proceed with long enough time that is comparable to the real experiment, which is at time scale of at least micro-second. However, a bio-system for study can contain thousands of particles, thus to keep essential topology of the system, simulation time is limited to nano-seconds due to restriction of computational power.

A compromising solution for such problem is to use coarse-graining–that is, to select atoms that share common chemical/biological characteristics,

then group them together and treat each group as a single bead. Clearly, such approximation will reduce degrees of freedoms of the original system, and ignore many inside interactions between the atoms. It is expected that such approximation might induce errors of simulation results. However, it turns out that, with clever choices of grouped atoms, coarse-grained models are able to generate simulation results that are in excellent agreements with experiments, while the time scale of simulation can be significantly extended to micro-seconds.

The MARTINI force field [47] is a popular coarse-grained molecular dynamics force field, which is suitable for biomolecular systems. It follows a simple four-to-one mapping, that is, four selected atoms are grouped and treated as one coarse-grained bead, and only polar, non-polar, apolar and charged interactions are defined in the force field. Some MARTINI mapping examples are visualized in Fig 2.1 [47].

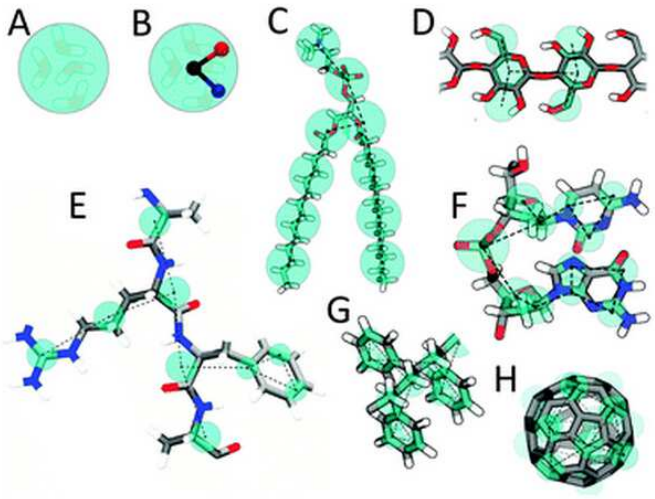

Figure 2.1: Martini mapping examples of selected molecules: (A) Standard water particle representing four water molecules, (B) Polarizable water molecule with embedded charges, (C) DMPC lipid, (D) Polysaccharide fragment, (E) Peptide, (F) DNA fragment, (G) Polystyrene fragment, (H) Fullerene molecule.

2.2 GROMACS: the MD Simulation Engine

Among currently available simulation packages of molecular dynamics, GROMACS (GROningen MAchine for Chemical Simulations)[6] is known for being lightweight, fast, free and open source. As an efficient engine to perform molecular dynamics simulations and energy minimization, GROMACS has various applications in computational biology and molecular modeling[6]. To accomplish a molecular dynamics simulation, GROMACS follows a four-step scheme to obtain the simulation results. In the following subsections, each of the four steps will be introduced in details.

2.2.1 Initialize GROMACS Files and Programs

GROMACS programs perform MD simulation steps by reading and writing files in several specific formats [69], which are listed below:

- xxx.mdp: the main parameter input file that records parameters and conditions for energy minimization, position restraints, and main MD simulation step
- xxx.pdb: short for the Protein DataBank file format,this input file contains molecular structure and coordinate information of the particles
- xxx.gro: similar to .pdb file, this input file contains molecular structure in Gromos 86 format, which indexes particles according to their types
- xxx.itp: an input topology file that defines the system particles' topologies, such as charge, mass, and radius of particles
- xxx.top: the input topology file, which defines the force fields, particle types and number of particles, its particles specifications are based on the .itp file
- xxx.tpr: the input file for simulation steps, it contains starting coordinates and velocities of the system particles
- xxx.xtc: the output file generated by production run, it includes trajectory information of all system particles for each time step
- xxx.edr: the output file generated by production run, it contains energy information at the end of simulation time

Furthermore, being a Unix-based program package, GROMACS command follows standard Unix/Linux command protocol, the most common functional routines are:

- mdrun: the main computational chemistry engine to perform molecular dynamics simulation and energy minimization
- editconf: a program that convert one file format to another
- grompp: before any production run, this program could take .top and .mdp file as inputs and generate the input file .tpr for the production run
- genbox: add solvants (water in most cases) into the coordinates file like .gro files
- g_msd: it takes .xtc file as input, and compute mean square displacement from the trajectory file, thus to compute diffusion constant of specific particles

Initial Conditions

Before any MD simulation, the topology file (.itp, .top) has to be properly edited, thus to load the force field, which defines the interactions between particles of the system. Then three parameters need to be initialized: coordinates and velocities of the particles, along with the pre-defined box size. These parameters will be included in .gro file. Setting initial velocities is optional, if velocities are not initialized manually, then GROMACS would assign initial velocities to the particles following MaxwellBoltzmann distribution in statistical mechanics [69], given temperature T:

$$p(v_i) = \sqrt{\frac{m_i}{2\pi BT}} exp(-\frac{m_i v_i^2}{2BT}) \tag{2.4}$$

where B is the Boltzman constant.

Periodic Boundary Conditions

One possible problem in molecular dynamics simulation is the "edge effect": the simulated particles in a system might move out of the pre-defined simulation box. To solve such problem, periodic boundary conditions are introduced into GROMACS, that is, the original single box is replaced by a box-array, which contains multiple translated copy of the same unit. For

the convenience of defining various systems, GROMACS allows different standard shapes for cell units (while for efficiency, rectangular cells are the most popular).

It is also worth noting that, to solve the problem that there are multiple particle images inside translated cells, GROMACS follows the so-called "minimum image" convention, that is, only the nearest particle image is considered for short-range non-bonded interactions. Specifically, a cut-off radius R_{cut} is applied to truncate short range non-bonded interactions, where R_{cut} is less than half the minimum box vector [69]:

$$R_{cut} < \frac{1}{2} min(||a||, ||b||, ||c||) \tag{2.5}$$

where a, b, c are the vectors defining the simulation box. The cut-off radius is set in the .mdp file.

Solvating the System

For the simulations of bio-systems, such as cell membrane, the whole system must be immersed into water to imitate a real bio-system. The program to add solvent water is "genbox". After solvating the system, topology files (.top) need to be edited to record the added water molecules. The number of added water molecules can be obtained by checking the output .gro file generated by genbox.

2.2.2 Energy Minimization

If initial state of the system (i.e initial velocities and positions of particles) is out of acceptable range, the force induced by the interactions will be too large for a simulation to start, due to a large value of potential energy. Thus a step of potential energy minimization is required to make sure the simulation can be started properly, as the system state will be close to equilibrium if its potential energy is approximately minimized.

This is a typical optimization problem that searches for the global minimum point of the potential function given by (2.3). There are numerous optimization algorithms (conjugate gradient, L-BFGS) available for energy minimization. In GROMACS, the most common one is the steepest descent method [69]. It chooses a step in the direction of the negative gradient, which guarantees the step to be descending, thus if the step size is proper, the global minimum point would be reached after enough steps of simulation.

To make sure all simulation steps start with a close-to-equilibrium state, energy minimization must be done whenever a system is changed (i.e after

a new system file is created or after solvents are added to a system). The parameters involved in energy minimization are defined in a specific .mdp file, which is basically same as the .mdp file used in production run, except that the "integrator" needs to be set to be "steep".

2.2.3 Running the Production Simulation

Once the system is well-equilibrated via energy minimization, it is ready for the production run of MD simulation. The program "grompp" records all the parameters in .mdp file to set the simulation in the desired environment, an example production run .mdp file containing common parameters is shown as follows:

$$
\begin{array}{ll}
integrator & =md \\
nsteps & =500 \\
dt & =0.002 \\
nstlist & =10 \\
rlist & =0.9 \\
coulombtype & =pme \\
rcoulomb & =0.9 \\
vdw-type & =cut-off \\
rvdw & =0.9 \\
tcoupl & =Berendsen \\
tc-grps & =protein \quad non-protein \\
tau-t & =0.1 \quad 0.1 \\
ref-t & =298 \quad 298 \\
Pcoupl & =Berendsen \\
tau-p & =1.0 \quad 1.0 \\
compressibility & =5e-5 \quad 5e-5 \\
ref-p & =1.0
\end{array}
\tag{2.6}
$$

This .mdp file initializes the simulation environment, such that equations of motion are integrated using the so-called leap-frog integrator ("$integrator = md$"), which is the default integrator in GROMACS, in 500 time steps with

0.002 ps for each step. "$nstlist = 10$" means the system is updated for every 10 steps, rlist is the cut-off distance (in nm), beyond which short-range non-bonded interactions for a certain particle would be ignored. Similarly, "rcoulomb" and "rvdw" set the cut-off distance for coulomb force and van der waals interactions, with units in nm. "coulomtype" defines the summation method used to calculate total energy of long range electrostatics, for more details, reader can refer to [69]. The rest of above parameters involve a concept of temperature and pressure coupling in GROMACS, which is introduced as follows.

Groups: Temperature and Pressure Coupling

Generally there are four types of ensembles for simulation of bio-systems:

- NVE: Constant number of particles (N), system volume (V) and energy (E)
- NVT: Constant number of particles (N), system volume (V) and temperature (T)
- NPT: Constant number of particles (N), system pressure (P) and temperature (T)
- NAP$_{xy}$T: Constant number of particles (N), system area (A), system pressure (P) along x-y direction, and temperature (T)

Since isothermal and isobaric simulations (NPT) are the most relevant to experimentl data, the temperature and pressure should be controlled properly in simulations. However, due to a result of integration errors and heating effects from interactive forces, temperature and pressure tend to drift slightly inside the simulated system. To solve such problems, GROMACS allows user to define groups to control the temperature and pressure.

For example, in the .mdp file presented in 2.6, two particle groups "protein" and "non-protein" are pre-defined, thus temperature-coupling and pressure-coupling algorithms can be applied to control the desired temperature/pressure. The most common coupling algorithm is the Berendsen weak coupling [69], it corrects the deviation of temperature T and pressure P with rates according to:

$$\frac{dT}{dt} = \frac{T_0 - T}{\tau_t} \quad \frac{dP}{d} = \frac{P_0 - T}{\tau_p} \tag{2.7}$$

where T_0, P_0 are the reference temperature and pressure, τ_t and τ_p are predefined constants for correction, with units in ps.

2.2.4 Analysis of the Simulation Results

The production run will output the trajectory file (.xtc) to record all the system state in each time step, and energy file (.edr) that contains all the energy terms at the end of simulation. With these information as a function of time, various system properties such as diffusion coefficient, thickness, surface tension and line tension of membrane can be obtained. Visualization tools such as pymol and VMD [31] can be used to visualize simulation results. Although output files can be processed and analyzed by any user-defined program, GROMACS offers various programs to analyze the simulation results. For example, g_msd can obtain mean square displacement of particles, which is used to calculate diffusion coefficients. g_energy can extract potential energy information, thus to calculate line tension and surface tension of a membrane system.

2.3 Summary

In this chapter, the global MD algorithm is explained using classical Newtonian physics equations. A coarse grained MARTINI force field is introduced in details. The MD simulation engine GROMACS is discussed by introducing its commonly used files and programs, along with details of configuration. Then a four-step scheme of MD simulation is introduced:

- Set up GROMACS files and programs with proper initializations
- Minimize potential energy to ensure the system start at a near-equilibrium state
- The production run simulation with configured .mdp file
- Analysis of the simulation results using various tools

As shown in next chapter, although CGMD simulation applies quite simplified physics to particles of a bio-system, by following the above four steps in GROMACS, the obtained simulation results are in excellent agreements with experimental measurements.

Chapter 3

Study of Cholesterol in Tethered Membranes

3.1 Introduction

As a major sterol component in most eukaryotic membranes, Cholesterol ($C_{27}H_{45}OH$) is an important membrane components, which can regulate membrane properties, such as lipid diffusion and membrane stability [34, 49]. Although significant research work has focused on the effects that cholesterol has on eukaryotic membranes, little attention has been paid to how cholesterol affects the properties of archaebacterial membranes. The aim of this chapter is to present a study of cholesterol on a multicomponent synthetic archaebacterial membrane, where CGMD simulation makes crucial contribution to justify the experimental results.

From coarse-grained molecular dynamics simulation, it can be shown that archaebacterial membrane properties including electroporation, diffusion dynamics, and biomechanics, are all affected by the concentration of cholesterol present in cell membrane. The experimental data also confirms the simulation results. Given the unique structure of archaebacterial lipids (i.e. the hydrocarbon chains are fictionalized with methyl groups), the cholesterol content has a noticeably different effect on the membrane properties compared to that of eukaryotic and prokaryotic membranes. The results provide novel insights into how cholesterol affects archaebacterial membrane properties, which are of use for the design of synthetic biomimetic membranes [57].

Related Works

Studies of cholesterol span over the past several decades, and have involved both experimental measurements and molecular dynamics techniques. For a review the reader can be referred to [34, 49] and citations therein. Due to the microscopic scale of length and time involved in membrane research, atomistic-level simulations are necessary for predicting the dynamic proper-

ties of membranes, which are difficult to be measured experimentally. Significant insights have been gained based on the use of molecular dynamics simulations. In [5, 10, 17, 52] it is shown that increasing the cholesterol content in POPC, DOPC, DSPC, and DPPC membranes will result in an increase in membrane stability, that is, an increasing physical resistance to membrane defects. While increasing the cholesterol in DOPC membranes reduces the membrane line tension [7]. In DPPC membranes, increasing the concentration of cholesterol will cause an increase in membrane thickness, and a decrease in the lateral diffusion of lipids [5, 25].

Recently coarse-grained molecular dynamics (CGMD) has been applied to study the atomistic effects cholesterol has on POPC, DOPC, and DPPC membranes [15]. The CGMD results show that for cholesterol concentrations between 0% to 40% the membrane thickness decreases, however for 50% the membrane thickness increases:possibly as a result of the interdigitation between lipid tails resulting from the free space under cholesterol [15]. So far a substantial amount of work has focused on lipids containing PO, DO, DS, and DP lipid tails. However, an important question is, what effects does cholesterol have on lipids with phytanyl tails, which are typically found in acrhaebacterial membranes? By using experimental measurements from black lipid membranes, Uitert *et. al.* [68] show that low concentrations of cholesterol increase the membrane stability, however above 20% the membrane stability begins to decrease. Several questions remain of how cholesterol affects the dynamics and biomechanics of archaebacterial membranes composed of phytanyl lipids.

Recent related works are summarized in Fig. 3.1.

Lipid Type	Simulation Method	Diffusion	Stability	Thickness	Reference
POPC	MD&CGMD	Decrease	Increase	No effects	[1,5]
DOPC	MD&CGMD	Decrease	Increase	N/A	[2,5]
DSPC	MD	Decrease	N/A	Increase	[3]
DPPC	MD&CGMD	Decrease	Increase	Increase	[1,4,5]

Figure 3.1: A brief summary of recent related works on study of cholesterol in membrane using MD/CGMD simulation methods

Simulation Setup and Key Results

In this thesis a CGMD model based on the MARTINI force field [45, 46] is constructed to study the diffusion dynamics and biomechanics of archaebacterial membranes containing cholesterol, whose concentrations range from 0% to 50%. The archaebacterial membrane is composed of 70% DphPC and 30% GDPE lipids (both of which contain phytanyl tails). Furthermore, to simulate a tethered archaebacterial membrane, two bioelectronic gold surface attaching membrane are included in the CGMD model. In Fig. 3.2, the brief ball structures of Dphpc, GDPE and cholesterol are provided, we can observe that compared with Dphpc and GDPE lipids, cholesterol is smaller in size.

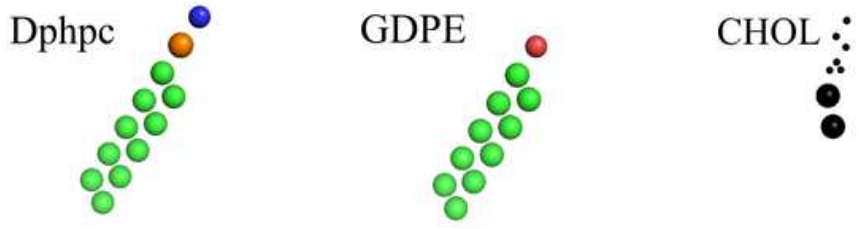

Figure 3.2: Ball structures of Dphpc, GDPE lpids, and Cholesterol

First, the CGMD simulation results are used to compute the membrane properties such as: diffusion dynamics of lipids, membrane thickness, surface tension, and line tension of the archaebacterial membrane. In [19], it was shown that lipids undergo three primary regimes of diffusion: the ballistic, subdiffusion, and Fickian diffusion. By using the results from mode-coupling theory and CGMD simulations, it will be shown that the transition time between the subdiffusion and Fickian diffusion regimes is not dependent on the concentration of cholesterol in the membrane. Therefore, the cholesterol only affects the diffusion coefficient of lipids in the Fickian diffusion regime. To validate the CGMD simulation results, we use experimental measurements from tethered archaebacterial membranes containing different concentrations of cholesterol.

Second, to ensure that the tethers and bioelectronic interface would not affect the membrane response, we must be able to compute the position dependent density of water at the bioelectronic interface. The fact that density has negligible variations at the membrane surface suggests that the bioelctronic interface does not impact the dynamics: this result is validated using diffusion measurements of the lipids in the distal and proximal layer

of the archaebacterial membrane. Additionally, by using approximations to the Yvan-Born-Green integral equation [72], we will show that harsh repulsive forces play a negligible role in the long range dynamics of the position dependent density profile of water at the bioelectronic interface.

Finally, in order to link the microscopic molecular dynamics simulation results and macroscopic experimental results, a fractional order macroscopic model is introduced. Experimental measurements are performed by measuring the current response of the tethered archaebacterial membranes to a given voltage excitation.

3.2 CGMD Simulation Setup and Membrane Formation

To investigate the effects of Cholesterol on archaebacterial membranes, a CGMD model of an archaebacterial membrane containing cholesterol is constructed. By using the MARTINI force field [45, 46] in simulation, the dynamics of lipid diffusion, membrane thickness, surface tension, and line tension will be studied. The CGMD model is validated by experimental measurements from a tethered archaebacterial lipid membrane, while a fractional order macroscopic model is to be introduced, thus to allow experimental results to be compared with simulation results. The CGMD model, along with the experimental measurements, provides key insights into how cholesterol and the bioelectronic interface impact the dynamics and biomechanics of archaebacterial membranes.

3.2.1 CGMD Model

To model the tethered archaebacterial membrane, we use the MARTINI force field [45, 46], which is a popular CGMD force field designed for biomolecular systems. The main set-up of the MARTINI force-field is to map approximately four heavy non-hydrogen atoms into one coarse-grained bead. Normally, each bead has a mass of 72 amu. For example, in the CGMD model four water atoms are represented by a single coarse-grained bead. To keep the model as simple as possible, only four main interactions are defined: polar (P), non-polar (N), apolar (C) and charged (Q), each of them has several subtypes. Q and N types have four subtypes, Q_{da}, Q_d, Q_a, Q_0 and Nda, Nd, Na, N0, which mean they have different hydrogen-bonding capabilities of the atom group: da = donor or acceptor, d = donor, a = acceptor, 0 = no hydrogen bonding. On the other hand, P and C types

have five subtypes, P_1, P_2, P_3, P_4, P_5 and C_1, C_2, C_3, C_4, C_5, where the subscripts 1-5 denote their increasing polar affinity [45, 46].

The CGMD model is constructed to imitate the essential dynamics of the tethered archaebacterial membrane system, which is composed of lipids, cholesterol, a gold bioelectronic interface, tethers and spacers. Given the fact that tether density of the tethered archaebacterial membrane is only about less than 1% (i.e. for every 268 lipid in the proximal layer one is tethered), the contribution of the tethers and spacers is regarded to be negligible, and therefore the tethering is not included in the CGMD model. The mapping of the lipids and gold surface into the MARTINI force field is provided as follows:

Lipids: The molecular components include the zwittrionic C20 diphytanyl-ether-glycero-phosphatidylcholine lipid (DphPC), C20 diphytanyl-diglyceride ether lipid (GDPE), cholesterol, and the gold surface. The tethered archaebacterial membrane we consider is composed of a 30% GDPE to 70% DphPC ratio of lipids. The lipid ratio is identical to that used for the experimental measurements. The phosphatidylcholine headgroup of the DphPC lipid is represented by two beads: the positive choline by the Q_0 bead, and the negative phosphate by the Q_a bead. The ether-glycol is represented by a SN_a bead, and each of the phytanyl tails by four C_1 beads.The phytanyl and either glycerol moieties of GDPE are represented by the same mapping as for the DphPC, however the hydroxyl headgroup of GDPE is represented by a P_4 bead. In total the DphPC lipid is composed of 12 beads, and the GDPE lipid by 11 beads. The cholesterol is represented by 8 beads as defined in [15].

Gold Surface: The gold surface is composed of a square lattice with custom P_f beads. The distance between adjacent beads is 0.3 nm. The interaction of the P_f bead is designed to reduce the effects of excess adsorption to the surface. The interaction between P_f and P_4 is 1/3 the value between P_4 and P_4, and the interaction between P_f and other bead types is $\sim$ 12% of the MARTINI value between P_4 and respective bead types. The following interactions are excluded: interaction between P_f beads, and between the C_5 beads of the tethers and spacers, and P_4 and Q_o beads of the lipids. Note that a similar interaction is used in [43] to represent the gold surface in the MARTINI force-field.

The complete CGMD simulation structure is provided in Fig.3.3 for reference. The tethering reservoir is selected to have a height of 4 nm to match the experimentally measured tethering reservoir thickness from [23].

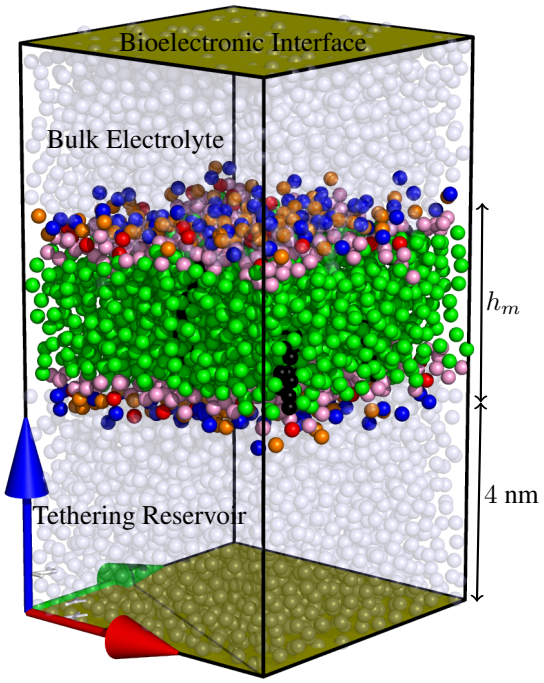

Figure 3.3: Coarse grained molecular dynamics structure of 0% tethered DphPC membrane with h_m denoting the membrane thickness. Lipid tails are represented by the green beads, Q_a bead is displayed in blue, the Q_o bead in orange, P_4 hydroxyl headgroup of GDPE by the red bead, the SN_a bead as pink, and the water beads as a translucent blue. The gold surface is indicated by the gold planes. Cholesterol is represented by the black beads. The coloring scheme of the axis is red for x, green for y, and blue for z.

3.2.2 Coarse-Grained Molecular Dynamics Simulation Protocol

The molecular dynamics simulations were performed using GROMACS [24] version 4.6.2 with the MARTINI force field [45, 46]. The interactions of the CGMD beads are defined by the Lennard-Jones (LJ) potential, and harmonic potentials (constraints=none) are utilized for bond and angle interactions. A shift function is added to the Coulombic force (coulombtype=shift) to smoothly and continuously decay to zero from 0 nm (rcoulomb-switch) to 1.2 nm (rcoulomb). The LJ interactions were treated likewise except that the shift function was turned on between 0.9 nm (rvdw-switch) and 1.4 nm

(rvdw). The grid-type neighbour searching algorithm is utilized for the simulation, that is, atoms in the neighbouring grid were updated every 10 time steps. The equations of motion are integrated using the leapfrog algorithm with a time step of 0.02 ps. Periodic boundary conditions are implemented in xy-dimensions (Fig. 3.3). Simulations are performed in the NAP_zT ensemble using a temperature of 350 K to match that used in [43] for similar membrane structures. The temperature is held constant using a velocity rescaling algorithm [9] with a time constant of 0.5 ps. Furthermore, Berendsen pressure coupling was applied with semi-isotropic type. The lipid and water molecules are coupled separately for temperature and pressure control. The gold surface is modeled using the *walls* option in GROMACS. Note that CGMD simulation times are reported as effective time, that is, four times the actual simulation time. The effective time is introduced to account for the speed-up in the CGMD model [45, 46].

All the systems studied here were first energy minimized using the steepest descent method in GROMACS. A 50 ns equilibration run is performed prior to the production run. Production runs are performed for a simulation time of up to 1 μs. Visualization of the CGMD results are reported using PyMOL.

3.2.3 Formation of Membrane in Experiment

The tethered archaebacterial membrane is constructed using the solvent-exchange formation process presented in [28,29]. The tethered membrane is supported on a polycarbonate slide containing a 100 nm thick sputtered gold electrodes each with dimensions 0.7×3 mm. The formation of the tethered membrane proceeds in two steps.

First, benzyl disulfide tetra-ethyleneglycol and benzyl disulfide tetra-ethyleneglycol are fixed to the surface of the gold electrode. Specifically, an ethanolic solution containing 370 μM of 1% benzyl disulfide tetra-ethyleneglycol and 99% benzyl disulfide tetra-ethyleneglycol is exposed to the gold surface for 30 min, then the surface is flushed with ethanol and air dried for approximately 2 min.

The second stage involves the formation of the tethered archaebacterial membrane. 8 μL of 3 mM ethanolic solution containing a mixture of 70% DphPC (zwitterionic C20 diphytanylether-glycerophosphatidylcholine) and 30% GDPE (C20 diphytanyl-diglyceride ether) lipids, and the rest cholesterol is brought into contact with the gold surface from the first step. This solution is incubated for 2 min at 20°C in allowing the formation of the tethered archaebacterial membrane. Proceeding the 2 min incubation, 300

μL of phosphate buffered saline solution at a pH of 7.2 is flushed through the chamber.

The tethered archaebacterial membrane is equilibrated for 30 min prior to performing any experimental measurements. The quality of the tethered archaebacterial membrane is measured continuously using an SDx tethered membranes tethaPodTM swept frequency impedance reader operating at frequencies of 1000, 500, 200,100,40,20,10,5,2,1,0.5,0.1 Hz and an excitation potential of 20 mV (SDx Tethered Membranes, Roseville, Sydney).

3.3 Laterial Diffusion Dynamics of Lipids and Cholesterol

The diffusion dynamics of a homogeneous medium like water can be described using standard Fickian diffusion, where the mean-square displacement (MSD) is proportional to time:

$$MSD = \langle (x(t) - x_0)^2 \rangle = 4Dt \tag{3.1}$$

Here x_o is the initial position, $x(t)$ is the current position at time t, D is the diffusion coefficient and $\langle \cdot \rangle$ is the ensemble average, the ensemble is taken over all particles.

However, as a result of the polymeric structure of lipids, the dynamics of lipids are more complex than simple liquids like water. Recently the so-called Mode-coupling theory (MCT), which is originally used for investigating dynamics of glass-forming liquids, has been applied to describe the diffusion dynamics of lipids in membranes [19]. In this section, we provide a method to model the diffusion dynamics of lipids, to see if the lipids are in the ballistic, subdiffusion, or Fickian diffusion regimes, by using the results from CGMD simulations

As predicted by MCT theory, the time evolution of the mean-square displacement of lipids is given by a generalized form of Fickian diffusion:

$$\langle (x(t) - x_o)^2 \rangle \propto t^{\beta} \tag{3.2}$$

where β is the power-law exponent. For standard Fickian diffusion $\beta = 1$, in which case the proportionality constant in Eq. 3.2 is related to the lipid diffusion coefficient D by ht Einstein relation $D = \langle (x(t) - x_o)^2 \rangle / 4t$.

The MCT theory [12] predicts that at the femtosecond timescale, the lipids are in a ballistic regime where $\beta = 2$. As time evolves, the lipids enter the subdiffusive region, with $\beta < 1$, as a result of local caging effects from

neighboring aggregated lipids. Then at the nanosecond timescale, the lipids enter the Fickian diffusion regime with $\beta = 1$, allowing for the diffusion coefficient to be computed as in Eq. 3.1. An estimate of the power-law coefficient β in Eq. 3.2 can be computed from the CGMD simulation trajectories using the following relation:

$$\beta(t) = \frac{\partial \ln(\langle (x(t) - x_o)^2 \rangle)}{\partial \ln(t)}. \tag{3.3}$$

To model the diffusion dynamics of the lipids, we consider the dynamics to satisfy the following linear Volterra integro-differential equation, which describes the time dependence of MSD in lipid bilayers [19]:

$$\begin{aligned} &\frac{\partial \langle (x(t))^2 \rangle}{\partial t} + \int_0^t M(t-s)\langle (x(s))^2 \rangle ds = 4(\frac{k_B T}{m_L})t, \\ &M(t) = \frac{\delta(t)}{\tau_3} + \frac{B e^{-t/\tau_1}}{(1 + (t/\tau_2)^{\overline{\beta}})}, \end{aligned} \tag{3.4}$$

for $x_o = 0$.

where $M(t)$ is the memory kernel, k_B is Bolztmann's constant, T is temperature, m_L is the mass of the lipid, and $\tau_1, \tau_2, \tau_3, \overline{\beta}$ and B are model parameters. τ_3 is the transition time at which the MSD transitions from the ballistic region to subdiffusion region, τ_2 the onset of the subdiffusion region, and τ_1 the transition from subdiffusion to Fickian diffusion region. The diffusion coefficient D can be computed from the results of Eq. 3.4 in the Fickian diffusion region, where for $t \to \infty$ the diffusion coefficient is related to the MSD by $\langle (x(t))^2 \rangle \approx 4Dt$, and can be evaluated using:

$$D = (\frac{k_B T}{m_L})\Big[\int_o^\infty M(t)dt\Big]^{-1}. \tag{3.5}$$

Notice that Eq. 3.5 provides another method to compute the diffusion coefficient D compared to the standard Eienstein relation given below Eq. 3.2.

3.3.1 Numerical Solution of Volterra Differential-Integral Equation

Although to our best knowledge, there is not any efficient method to solve Eqn. 3.4 analytically, it is still possible to obtain an approximate numerical

solution, where numerical differentiation and numerical integration can be calculated by using finite difference method:

$$f'(t) \approx \frac{f(t+h) - f(t)}{h} \tag{3.6}$$

where the subdivided interval of integration h is represented by:

$$h = \frac{t_N - a}{N} \tag{3.7}$$

here N is the number of subdivided intervals chosen and t_N is the last time step. Similarly, t_i is the i^{th} time step. Then by using the trapezoidal rule:

$$\int_0^{t_n} f(x) \approx h(\frac{1}{2}(f(x_1) + 2[f(x_2) + f(x_3) + ...f(x_{n-1})] + \frac{1}{2}f_n) \tag{3.8}$$

and simpson's rule:

$$\begin{aligned}\int_0^{t_{2n}} f(x)dx \approx &\frac{h}{3}[f_0 + 4(f_1 + f_3 + ... + f_{2n-1}) + \\ &2(f_2 + f_4 + f_{2n-2}) + f_{2n}]\end{aligned} \tag{3.9}$$

the integration term in volterra integral-differential equation 3.4 can be approximated by plugging in trapezoidal rule and simpson's rule for odd and even time steps, respectively, then clearly we have the approximated integrals for each time step:

$$\begin{aligned}\int_0^{t_1} M(t-s)\langle(x(s))^2\rangle ds \approx &h[\frac{1}{2}M(t_1 - s_1)\langle(x(s_1))^2\rangle] \\ \int_0^{t_2} M(t-s)\langle(x(s))^2\rangle ds \approx &\frac{h}{3}[M(t_2 - s_0)\langle(x(s_0))^2\rangle ds + \\ &4M(t_2 - s_1)\langle(x(s_1))^2\rangle ds + \\ &M(t_2 - s_2)\langle(x(s_2))^2\rangle ds]\end{aligned}$$

$$
\begin{aligned}
\int_0^{t_3} M(t-s)\langle(x(s))^2\rangle ds \approx & h[\frac{1}{2}M(t_3-s_0)\langle(x(s_0))^2\rangle ds+ \\
& M(t_3-s_1)\langle(x(s_1))^2\rangle ds+ \\
& M(t_2-s_2)\langle(x(s_2))^2\rangle ds+ \\
& \frac{1}{2}M(t_3-s_3)\langle(x(s_3))^2\rangle ds] \\
& \cdots\cdots \\
\int_0^{t_{N-1}} M(t-s)\langle(x(s))^2\rangle ds \approx & h[\frac{1}{2}M(t_{N-1}-s_0)\langle(x(s_0))^2]+ \\
& M(t_{N-1}-s_1)\langle(x(s_1))^2]\rangle ds+... \\
& M(t_{N-1}-s_{N-2})\langle(x(s_{N-2}))^2]\rangle ds+ \\
& \frac{1}{2}M(t_{N-1}-s_{N-1})\langle(x(s_{N-1}))^2]\rangle ds \\
\int_0^{t_N} M(t-s)\langle(x(s))^2\rangle ds \approx & \frac{h}{3}[M(t_N-s_0)\langle(x(s_0))^2\rangle ds+ \\
& 4[M(t_N-s_1)\langle(x(s_N))^2\rangle ds+... \\
& M(t_N-s_{N-1})\langle(x(s_{N-1}))^2\rangle ds] \\
& 2[M(t_N-s_1)\langle(x(s_N))^2\rangle ds+... \\
& M(t_N-s_{N-2})\langle(x(s_{N-2}))^2\rangle ds]+ \\
& M(t_2-s_2)\langle(x(s_2))^2]\rangle ds
\end{aligned}
\tag{3.10}
$$

So if we re-write the above approximated representations in a more compact form, that is, if we rename $M(t_i-s_j)$ to be M_{ij}, and rename $\langle(x(s_j))^2]\rangle$ to be x_j, then the numerical volterra integral-differential equation 3.4 can be written as:

$$
\begin{aligned}
\frac{x_2-x_0}{2h} =& 4\frac{k_BT}{m_L}t_1-\frac{h}{2}[M_{10}x_0+M_{11}x_1] \\
\frac{x_3-x_1}{2h} =& 4\frac{k_BT}{m_L}t_2-\frac{h}{3}[M_{20}x_0+4M_{21}x_1+M_{22}x_2] \\
& \cdots\cdots \\
\frac{x_N-x_{N-2}}{2h} =& 4\frac{k_BT}{m_L}t_{N-1}-\frac{h}{2}[M_{N-1,0}x_0+ \\
& 2[M_{N-1,1}x_1+...M_{N-1,N-2}x_{N-2}]+M_{N-1,N-1}x_{N-1}]
\end{aligned}
$$

$$\frac{x_N - x_{N-1}}{2h} = 4\frac{k_B T}{m_L} t_N - \frac{h}{3}[M_{N0}x_0 + 4[M_{N1}x_1 + ...M_{N,N-1}x_{N-1}] + 2[M_{N2}x_2 + ...M_{N,N-2}x_{N-2}] + M_{N,N}x_N] \tag{3.11}$$

Therefore the Eqn 3.11 can be re-written in a matrix form $AX = B$, where $X = [x_1, x_2, ...x_N]'$, and

$$A = \begin{bmatrix} h^2 k_{11} & 1 & 0 & \dots & 0 \\ 0 & \frac{8h^2}{3}k_{21} + \frac{2h^2}{3}k_{22} - 1 & 1 & \dots & 0 \\ \dots & \dots & \dots & \dots & \dots \\ 0 & \dots & A_{N-1,N-2} & 1 & 0 \\ 0 & 0 & \dots & A_{N,N-1} & 1 \end{bmatrix} \tag{3.12}$$

with

$$A_{N-1,N-2} = 2[h^2 M_{N-1,1} + ...h^2 M_{N-1,N-2}] + h^2 M_{N-1,N-1}$$

and

$$A_{N,N-1} = \frac{8h^2}{3}[M_{N1}+M_{N3}+...M_{N,N-1}]+\frac{4h^2}{3}[M_{N2}+M_{N4}+...M_{N,N-2}]+\frac{2h^2}{3}M_{NN}$$

Furthermore,

$$B = \begin{bmatrix} 8h\frac{k_B T}{m_L}t_1 - h^2 M_{10}x_1 + 1 \\ 8h\frac{k_B T}{m_L}t_2 - \frac{2h^2}{3}M_{20}x_2 \\ 8h\frac{k_B T}{m_L}t_3 - h^2 M_{10}x_3 \\ . \\ . \\ . \\ 8h\frac{k_B T}{m_L}t_{N-1} - h^2 M_{N-1,0}x_{N-1} \\ 8h\frac{k_B T}{m_L}t_N - \frac{2h^2}{3}M_{N0}x_N \end{bmatrix} \tag{3.13}$$

Now we are able to solve the matrix equation $AX = B$ and obtain the mean-square displacements as a function of time. Thus the ballistic, subdiffusive and Fickian region can be observed. However, as mentioned above, the ballistic region and subdiffusive region will occur at timescale of femtosecond, or 10^{-6} nanosecond. This means that if we require a 1 ms computation, the dimension of matrix A is at least $10^9 \times 10^9$. Although A is a sparse matrix, still the required computational power and time for solving this equation is considered to be excessive. Further work of matrix sparsification is expected to be done regarding this part. Since in this thesis, we are only considering the effects of cholesterol on Fickian diffusion dynamics of membrane, CGMD simulation results are used to analyze the diffusion dynamics of lipids.

3.3.2 CGMD Simulation Results on Diffusion Dynamics

In this subsection, the results of CGMD simulations are utilized to gain insights into the concentration effects, that cholesterol has on the diffusion dynamics of lipids in the archaebacterial membrane.

The key question addressed in this section is to confirm that, if the lipid dynamics in CGMD model indeed shows a short time ballistic regime, an extended subdiffusion regime, and a Fickian diffusion regime, as predicted by the MCT theory. Furthermore, if these regimes are present, then what is the transition time between each regime. Knowledge of these transition times is crucial, as based on Eq. 3.1, the diffusion coefficients can only be computed using CGMD trajectories in the Fickian diffusion regime.

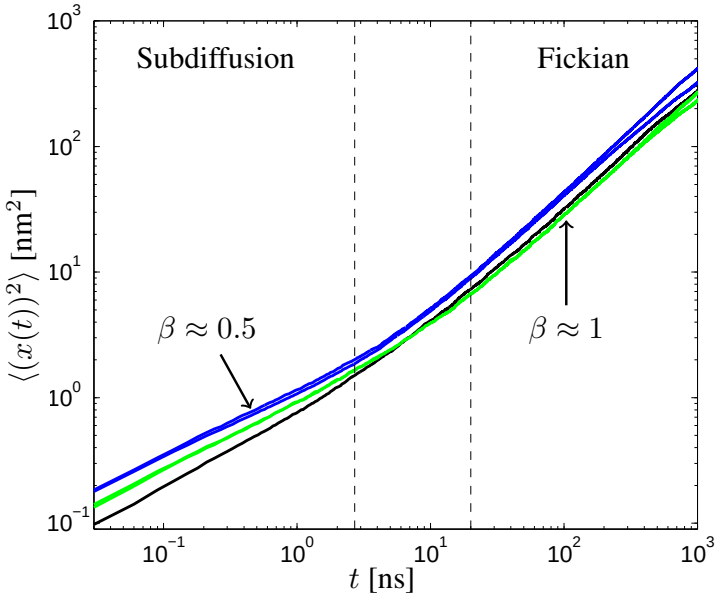

Figure 3.4: Computed mean-square displacement for the DphPC, GDPE, and cholesterol for the 0% and 50% cholesterol membranes with β define in Eq. 3.3. Notice that the diffusion dynamics are in the subdiffusion regime ($\beta \approx 0.5$) for $t \leq 3$ ns, and for $t \geq 20$ ns the diffusion dynamics are in the Fickian regime ($\beta \approx 1$) . This is in agreement with the mode-coupling theory for flexible macromolecules [11, 19].

Fig. 3.4 presents the numerically computed mean-square displacement of DphPC, GDPE, and cholesterol from the CGMD simulation results for cholesterol concentrations of 0% and 50%, which are generated from the

trajectory .xtc file of simulation. From Fig.3.4, we see that for $t \leq 3$ ns the molecules diffuse in the subdiffusion regime, and for $t \geq 20$ ns the diffusion of the molecules is in the Fickian diffusion regime. This is in agreement with the results predicted using mode-coupling theory for flexible macromolecules [11, 19]. Given the time step of the CGMD simulation is 20 fs, the ballistic region $\beta > 1$ is not observed in Fig. 3.4 for any of the lipids or cholesterol. This is expected as the ballistic region is typically observed for $t \leq 10$ fs [19].

Surprisingly, the transition times between the subdiffusion and Fickian diffusion regime is not dependent on the cholesterol content. This suggests that the concentration of cholesterol presented contributed negligibly to the caging effect, that is, only the Fickian diffusion dynamics are strongly dependent on the concentration of cholesterol present. The results in [18, 25] for SOPC, SLPC, SAPC, SDPC, and DPPC suggest that as the cholesterol content increases there should be a decrease in the diffusion coefficient D.

Table 3.1: Lipid and Cholesterol Diffusion ($nm^2/\mu s$)

	DphPC	GDPE	Cholesterol
0%	69.6±3.2	57.4±2.7	-
10%	69.0±0.4	56.3±2.4	106.5±40.9
20%	49.3±1.3	44.4±2.6	92.5±33.7
30%	50.0±3.8	48.5±1.2	86.8±29.1
40%	54.5±10	67.5±7.3	55.1±8.6
50%	39.5±1.6	31.3±1.8	46.7±8.2

To gain insight into how the concentration of cholesterol affects the diffusion dynamics in the Fickian regime, we compute the diffusion coefficient D for DphPC, GDPE, and cholesterol for archaebacterial membranes containing 0% to 50% cholesterol. The results are provided in Table 3.1. The diffusion coefficient of DphPC for 0% cholesterol is in excellent agreement with the experimentally measured diffusion coefficient of 18.1 ± 5.6 $nm^2/\mu s$ [4]. Furthermore, the numerically computed diffusion coefficient of cholesterol are in excellent agreement with the experimentally measured diffusion coefficient of cholesterol which are in the range of 10 $nm^2/\mu s$ to 100 $nm^2/\mu s$ [56, 63]. The cholesterol has a higher diffusion coefficient than DphPC and GPDE, and the diffusion of cholesterol monotonically decreases as the concentration of cholesterol increases. If we consider only the mass and size of cholesterol, it is expected that the lower mass and size of choles-

terol compared to DphPC and GDPE will allow cholesterol to have a larger diffusion coefficient. Another contributing factor is that the headgroup of DphPC and GDPE both have a larger dipole moment than that of cholesterol which will also reduce the diffusion coefficient of the lipids compared to the cholesterol [25].

An interesting question is, why a "slow" lipid system could be even slowed down by faster-moving cholesterol, which has higher diffusion coefficients than GDPE and Dphpc molecules? Such phenomenon can be well explained by the free volume theory [67], which is used to predict a liquid-ordered-liquid-disordered ($l_o - l_d$) coexistence region in phosphatidylcholine/cholesterol mixture [55]. If the environment temperature is above the phase transition temperature, the membrane lipids are in the so-called disordered phase (l_d), where the acyl chains of the phospholipid molecules are in a disordered state that contains a high fraction of gauche conformers [2]. When cholesterol are added into the membrane, cholesterol first span over the hydrocarbon cores of the bilayer, if concentration of cholesterol increases, free-volum models [54, 55] predict that excessive cholesterol would pack tightly into the lipids, thus the cavities and deflects from the membrane are filled by cholesterols, and more regions of membrane are converted into the ordered state (l_o), which has much less free volume, and therefore, smaller diffusion coefficients.

3.4 Water Density Profile at Bioelectronic Interface

Before conducting actual experimental measurements for the tethered membrane, a crucial problem is to figure out the region where the properties of tethered membrane are not affected by bioelectronic interface. Thus it becomes necessary that water density profile nearby the gold surface should be investigated: the membrane should be set in the region where water density profile is not affected much by the bioelectronic interface.

As the dynamics of water in proximity to the bioelectronic interface have very different characteristics from that in the bulk region [3, 21, 76], the thermodynamic and structural properties of water molecules at the interface are affected by two primary factors: a smaller number of neighboring molecule interactions, and a change in the potential energy of the fluid as a result of interactions with the surface. The density profile of water near the interface typically consists of oscillations that are similar to sinusoidal waves , with period close to the mean thickness of each water layer in proximity to the

interface [21, 76]. This observation suggests that the oscillations occur at a similar length scale to the molecular diameter of the water molecules.

In our simulation the interface is modeled using a lattice of coarse-grained beads which interact with the water beads via a Lennard-Jones potential. Then a key question we would like to answer is: does the density profile from the CGMD model match that from a hard-sphere fluid at a hard-wall interface? In this section we will show that, approximations to the Yvan-Born-Green integral equation [72], which lead to an analytical result represented by the so-called "Percus-Yevick Equation", will be able to evaluate the density profile of a hard-sphere fluid at a hard-wall interface. This density profile can then be compared with the density profile from the CGMD simulation, thus to evaluate the effects of harsh repulsive forces that CGMD water beads have on the water density.

Now let's provide a derivation of the Percus-Yevick equation first.

3.4.1 Derivation of Percus-Yevick Equation

First we consider a monoatomic fluid with density ρ, which is interacting with pair potential u, and an external potential ϕ that represents the contribution of interactions from the interface. Then the mean force acting on particle 1 by a particle 2 can be represented by the gradient of potential $-\nabla_1 u(r_1, r_2)$. The total mean force on particle 1 by the other particles and interface is given by the Yvan-Born-Green integral equation [72]:

$$\begin{aligned} k_B T \nabla_1 \ln(\rho(r_1)) = \\ -\nabla_1 \phi(r_1) - \int \nabla_1 u(r_1, r_2) \rho(r_2|r_1) dr_2 \end{aligned} \tag{3.14}$$

where k_B is the Boltzmann's constant, T is the temperature, and $\rho(r_2|r_1)$ the conditional singlet density (i.e. the conditional density at r_2 given a particle is fixed at r_1).

In (3.14) the so-called correlation function is represented as function of the external field ϕ. Note that the right hand side of (3.14) is the average force acting on a particle fixed at r_1. To estimate $\rho(r)$, approximations to (3.14) are to be made to only account for long-range interactions. The main idea is to construct an external reference potential ϕ_R, which only accounts for long range interactions of the particles and the interface, and pair interaction that only accounts for short range interactions, which is denoted as the reduced system. The only requirement is that the density profile of the full system and reduced system must be equal. Using this method, Weeks *et. al.* [72] propose the approximation that the singlet density for both the

full system and reduced system must be similar at short range. The external potential ϕ and reference potential ϕ_R are then related by [21, 72]:

$$\phi_R(r_1) = \phi(r_1) + \int [\rho_R(r_2) - \rho_B] u_1(r_1, r_2) dr_2 \tag{3.15}$$

with ρ_B the bulk density, $u_1(r_1, r_2)$ the attractive part of the pair potential, and ρ_R the density in the external reference potential. Note that for a given $\rho(r)$, which can be computed from the CGMD simulation, an effective reference potential ϕ_R can be evaluated by solving (3.15) self-consistently. To solve for $\rho(r)$ analytically we must determine an expression for ϕ_R in (3.15). It is reasonable (we will see why very soon) to approximate ϕ_R by $\phi_{R'}$ where we have neglected the harsh repulsive forces at the interface leaving only the attractive forces in the full system. Then, for a hard-wall, $\phi = \infty$ for $r \leq 1$ and 0 otherwise, the density $\rho(r)$ is given by [71]:

$$\begin{aligned} &\rho(r_1) = \rho_B + \rho_B \int [\rho(r_1) - \rho_B] c(r_{12}) dr_2, \\ &\rho(r_1) = 0 \text{ for } r_1 \leq 1 \end{aligned} \tag{3.16}$$

with $c(\cdot)$ the direct correlation function of the fluid, $r_{12} = r_1 - r_2$. For a hard-sphere, the direct correlation function is given by a cubic polynomial which is dependent on the radius of the hard-sphere, denoted by R, and the bulk water density ρ_B [73]. For a hard-sphere and hard-wall interface Eq. 3.16 is given by the Percus-Yevick equation which can be solved analytically using the method in [70], which is shown as follows.

The close form of Percus-Yevick equation is derived directly from Ornstein-Zernike equation, which simply states that total influence h of particle i on particle j is a superposition of both direct and indirect influence:

$$h(r_{ij}) = c(r_{ij}) + \rho_B \int dr_k c(r_{ik})[g(r_{kj}) - 1] = g(r) - 1 \tag{3.17}$$

where $g(r)$ is the "scaled" density of particles, or the pair distribution function; the direct correlation function $c(r_{ij})$ describes the direct influence of particle i on particle j; and second term of the equation, which is the indirect correlation function, suggests that the indirect influence of particle i on particle j is an integrated result of particle i acting on a reference particle k, which in turn has influence on j.

By assuming the case of hard sphere potential:

$$u(r) = \begin{cases} \infty & \text{if } r < b \\ 0 & \text{if } r \geq b. \end{cases} \tag{3.18}$$

where b is the radius of particle, after defining function $y(r)$ to be:

$$h(r) - c(r) = y(r) - 1,$$

with

$$y(r) = \begin{cases} -c(r) & \text{if } r < b \\ g(r) & \text{if } r \geq b. \end{cases} \tag{3.19}$$

it's straightforward to conclude that

$$c(r) = \begin{cases} -y(r) & \text{if } r < b \\ 0 & \text{if } r \geq b. \end{cases} \tag{3.20}$$

Then by setting particle j to be the original point, rename $r_i = r$, $r_j = r'$, we can express Ornstein-Zernike equation in terms of $y(r)$ [65]:

$$y(r) = 1 + \rho_B \int_{r'<b} dr' y(r')[1 - g(r - r')] \tag{3.21}$$

compared with Eq. 3.16, clearly they are equivalent if we set $\rho(r)/\rho_B = g(r)$.

Wertheim had obtained a close-form analytical solution for the P-Y equation. It was suggested that the solution for direct correlation function is actually a cubic polynomial:

$$-c(r) = \alpha + \beta(r/b) + \gamma(r/b)^3 \tag{3.22}$$

with

$$\alpha = \frac{(1+2f)^2}{(1-f)^4}, \beta = -6f\frac{(1+f/2)^2}{(1-f)^4}, \gamma = \frac{f(1+f)^2}{2(1-f)^4}, f = \frac{\rho_B \pi b^3}{6}$$

for $x \leq 1$, where f is defined as the fractional volume of the particle.

As the indirect correlation function in the Ornstein-Zernike equation is a convolution integral, then in Fourier Transform domain, it's proportional to the product of fourier transforms of h(r) and c(r), we could take advantage of this property.

$$\begin{aligned} H(p) &= \frac{1}{(2\pi)^3} \int_{-\infty}^{\infty} dr e^{-ip\cdot r} h(r) \\ C(p) &= \frac{1}{(2\pi)^3} \int_{-\infty}^{\infty} dr e^{-ip\cdot r} c(r) \end{aligned} \tag{3.23}$$

Solving the Ornstein-Zernike equation in Fourier Transform domain gives us:

$$H(p) = \frac{C(p)}{1 - \rho_B(2\pi)^3 C(p)}$$

Then by doing inverse fourier transform:

$$h(r) = \int_{-\infty}^{\infty} dp e^{ip\cdot t} H(p) = 4\pi \int_0^{\infty} dp(\frac{sinpr}{pr})p^2 H(p) \tag{3.24}$$

Finally, the pair distribution function g(r) is given by $g(r) = h(r) + 1$ [65].

3.4.2 Match the Percus-Yevick Equation with CGMD Results

Fig. 3.5 shows the water density profile from the CGMD simulation, along with the density profile predicted by the Percus-Yevick equation (Eq. 3.16). Notice that the two density profiles in Fig. 3.5 are in excellent agreement. Remember that the solution of Percus-Yevick equation 3.24 does not involve short-range interactions, this suggests that harsh short-range interactions in the LJ potential do not play a significant role in the density profile. The radius of the hard-sphere in the Percus-Yevick equation is $b = 0.495$ nm, which is in agreement with the potential well of the LJ potential of the CGMD water of 0.47 nm. As seen in Fig. 3.5, the distance between the local minima/maxima is approximately b, as expected from the discussion in [21, 76]. At 4 nm from the bioelectronic interface, there is negligible variation in the density profile, which suggests that the lipid diffusion coefficients should not be effected by the interface. To validate this claim, we computed the diffusion coefficients in the proximal and distal layers and found them to be in excellent agreement. For example, for the 20% cholesterol membrane the diffusion coefficients of the DphPC lipids in the proximal and distal layers are 49.1 ± 1.2 and 49.3 ± 1.3 nm$^2/\mu$s respectively.

Given the fact that bioelectronic interface is in close proximity (i.e. approximately 4 nm) to the membrane surface, we would like to investigate the effect that the bioelectronic interface have on the water dynamics and diffusion dynamics of lipids. Given the distance between the bioelectronic interface and membrane surface is 4 nm, with the investigations made above, we are able to show that the density variations are negligible at a distance of 4 nm from the interface. Indeed, we have successfully estimated that the negligible importance of harsh short range interactions of the water beads on the density profile. Therefore the bioelectronic interface contributes negligibly to the diffusion dynamics of the lipid membrane. Using

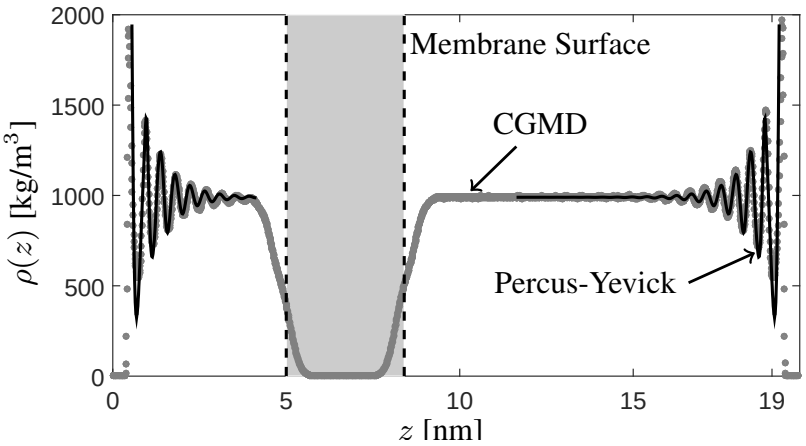

Figure 3.5: The computed water density computed from the CGMD simulation results, and analytical results from the Percus-Yevick equation (Eq. 3.16) with $R = 0.49$ nm and $\rho_B = 1000$ kg/m^3. The bioelectronic interface is located at $r = 0$ nm and $r = 19.8$ nm.

the Percus-Yevick equation (Eq. 3.16), it is shown that the long-range interactions of water dominate the density profile of the LJ fluid in the CGMD model.

3.5 Archaebacterial Membrane Biomechanics

How does the concentration of cholesterol affect the archaebacterial membrane biomechanics? By using the results from CGMD simulations, we study how cholesterol content affects membrane thickness h_m, line tension γ, and surface tension σ. Recall that the fractional order macroscopic model is dependent on h_m, γ, and σ, which allows experimental measurements from the tethered archaebacterial membrane to be utilized to validate the results from the CGMD model. The computed h_m, σ, and γ for the 0% to 50% cholesterol membranes is provided in Table 3.2.

3.5.1 Archaebacterial Membrane Thickness

Table 3.2 provides the numerically computed membrane thickness for % cholesterol from 0% to 50%. The membrane thickness for the 0% cholesterol is in agreement with the experimentally measured thickness for DphPC based tethered membranes, which do not contain cholesterol [23]. The position

Table 3.2: Biomechanic Parameters of Membrane

	0%	10%	20%	30%	40%	50%
Membrane Thickness h_m (nm)						
PO_4	3.8	4.09	4.13	4.17	3.92	3.61
OH	3.36	3.65	3.69	3.76	3.81	3.98
ROH	-	2.92	3.01	3.06	3.09	3.17
Surface Tension (mN/m)						
σ	57.8	73.5	86.1	97.1	68.9	43.9
Line Tension (pN)						
γ	50.8	51.8	54.8	60.5	69.4	70.1

The membrane thickness is computed from the distance between the molecule in the distal to the molecule in the proxyl layer of the membrane.

of cholesterol's hydroxyl group (ROH) is always less than the associated head groups (OH and PO_4) of the DphPC and GDPE. This is in agreement with the results from molecular dynamics simulation of DPPC molecules for 11% and 50% cholesterol [62]. As expected, as the cholesterol content increases from 0% to 30%, there is a decrease in membrane thickness as a result of the cholesterol forming a complex with the hydrocarbon tails. A similar effect has been observed for cholesterol in DPPC, DMPC, SOPC, and POPC membranes (6, 45, 46). Interestingly for archaebacterial membranes containing 40% and 50% cholesterol there is a decrease in membrane thickness. This results suggests that the phytanyl chains in the DphPC and GDPE form a complex with the cholesterol causing the membrane thickness to decrease. Note that this is similar to the condensing effect suggested for DPPC, DMPC, SOPC, and POPC membranes [17, 32, 66] in which the cholesterol forms a complex with the hydrocarbon tails. However, in the case of lipids with a phytanyl tail, there is a decrease in thickness not an increase.

To validate the numerically computed membrane thickness, we use experimental measurements from tethered archaebacterial membranes. Recall that the capacitance of the tethered membrane C_m is dependent on the dielectric permittivity ε_m, thickness h_m, and surface area of the membrane A_m. For a constant ε_m and surface area A_m fixed to be 2.1 mm^2, as h_m decreases the associated capacitance of the membrane must increase. From Table 3.3,as the concentration of cholesterol from 0% to 30% increases the

associated capacitance of the membrane decreases, this suggests that the membrane thickness is increasing. From 40% to 50% cholesterol concentration, the tethered membrane capacitance increases, this suggests a decrease in membrane thickness. These results validate the numerically computed archaebacterial membrane thickness provided in Table 3.2 for concentrations of cholesterol from 0% to 50%.

3.5.2 Archaebacterial Membrane Line Tension and Surface Tension

Before introducing the macroscopic model, methods of computing the line tension γ and surface tension σ based on CGMD simulation results are provided, because the calculation of membrane conductance will depend on the surface tension and line tension. The line tension γ is defined as the energy cost per unit length at the boundary, where the hydrocarbon lipid tails and water are splited. The surface tension σ is defined as the energy required to increase the surface area of the membrane by a unit area. Therefore, the defect density (instability) of the membrane increases as the ratio γ/σ increases.

To compute the line tension γ of the membrane, we use the procedure provided in [35]. The line tension can be computed from the ribbon like structure (Fig.3.6) using

$$\gamma = \frac{1}{2}\Big\langle L_x L_y \big[\frac{P_{xx} + P_{yy}}{2} - P_{zz}\big]\Big\rangle \tag{3.25}$$

with P_{xx}, P_{yy}, P_{zz} the diagonal elements of the pressure tensor, L_x and L_y the simulation size in the x and y directions respectively, and $\langle \cdots \rangle$ denoting the ensemble average over time.

To construct the lipid structure in (Fig. 3.6), an intact bilayer containing 320 lipids, with a 70% DphPC and 30% GDPE composition is used. The hydrophilic interior of the bilayer is initially adjacent to the x and z dimensions of the simulation cell. The simulation cell is then expanded in the x direction from 14 nm to 16 nm, and in the y direction from 10 nm to 13 nm to ensure the membrane forms an edge. Initially a 50 ns equilibration run was performed to allow the edge to form, this was followed by a 250 ns production from from which γ (3.25) can be estimated. Simulation are performed in a $NP_{xy}L_zT$ ensemble at a temperature of 320 K. Temperature is kept constant using the velocity rescaling algorithm [9] with a time constant of 0.5 ps. Pressure is coupled semi-isotropically using the weak coupling scheme [9] with a time constant of 3 ps, compressibility of 0.3 $\mathrm{nm}^2/\mathrm{nN}$, and a reference pressure of 100 $\mathrm{kN/m}^2$.

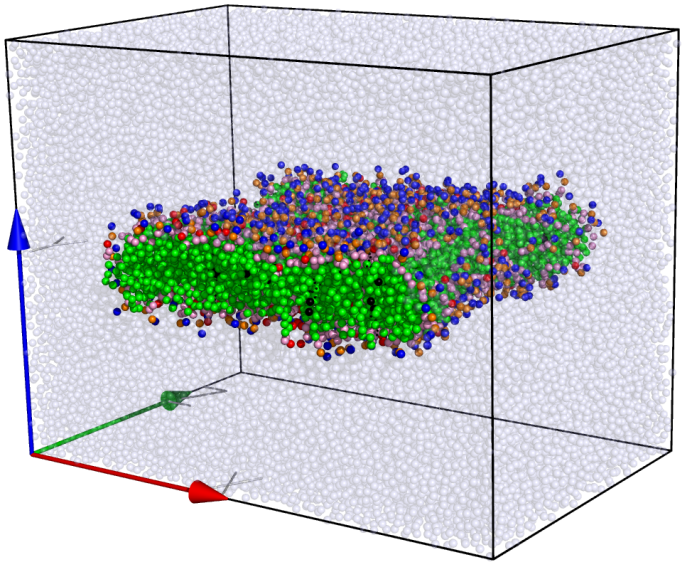

Figure 3.6: Ribbon structure of archaebacterial membrane. The bead coloring is identical to that used in Fig. 3.3. The coloring scheme of the axis is red for x, blue for y, and green for z. Note that this axis is only used for computing the line tension.

The surface tension of the membrane is computed using [35]:

$$\sigma = \frac{1}{2}\Big\langle L_z \big[P_{zz} - \frac{P_{xx} + P_{yy}}{2}\big]\Big\rangle \tag{3.26}$$

with the parameters defined below (3.25). The evaluation of (3.26) is performed in the $NAP_{xy}T$ ensemble using a total production run of 250 ns. From Table 3.2 the cholesterol content both affects the surface tension and line tension of the membrane. The computed values for the surface tension in Table 3.2 are in excellent agreement with the experimental results provided in [75], and simulation results from [36, 37, 74], whose work focus on similar DphPC based membranes. From molecular dynamics simulations of DPPC membranes, as the percentage of cholesterol increases there is a decrease in the surface area of the membrane [25]. Since the surface tension is defined as the energy required to increase the surface area of the membrane by a unit area, due to the interactions between cholesterol and lipids, if the concentration of cholesterol increases the surface tension of the membrane is expected to increase. From Table 3.2, for 0% to 30% cholesterol the surface tension σ increases with increasing cholesterol content. However, it is

unexpected that the surface tension decreases for 40% and 50% cholesterol content. Furthermore, from Table 3.2 we see that as the line tension γ of the membrane monotonically increases as the cholesterol content increases.

An interesting question is, why the line tension of the lipid/cholesterol mixture increases monotonically when concentration of cholesterol increases, while surface tension increased till 30% cholesterol, then dropped down afterwards? The process of raft formation over membrane surface is able to provide an explanation. As it has been well studied, when cholesterol is introduced into saturated phospholipids, a raft-like domain could be formed and enhanced as the concentration of cholesterol increases [64]. Since surface tension is defined as the energy cost per unit area associated with decreasing the membrane area, when small clusters of cholesterol formed, a gradually ordered state of phospholipid/cholesterol mixture is stabilized, thus surface tension increases. However, if the concentration of cholesterol is very high (above 30%), small clusters of cholesterol are expected to collide with each other to form larger ones, thus the whole system is again de-stabilized by large clusters and surface tension decreases. Furthermore, for the line tension case, Equation . 3.25 showed that line tension represents a force along one direction (in our case, the zz-direction in Fig. 3.6), thus when more raft structures form on the membrane, more ordered states are introduced along zz-direction, thus line tension increases monotonically.

To validate the computed surface tension σ and line tension γ in Table 3.2 we use experimental results from tethered archaebacterial membranes. Recall that the population of membrane defects increases as the ration γ/σ increases. The population of membrane defects is given by the equilibrium membrane conductance G_m, which can be measured experimentally from the fractional order macroscopic model. From the experimentally measured membrane conductance G_m in Table 3.3, for 0% to 30% cholesterol the ratio γ/σ is expected to decrease, and from 40% to 50% γ/σ is expected to increase. This result is in agreement with the numerically computed σ and γ in Table 3.2.

3.6 Fractional Order Macroscopic Model

In this section the fractional order macroscopic model of the tethered archaebacterial membrane is to be provided. Experimental measurements from the tethered membrane and macroscopic model are used to validate the results from the CGMD model. The tethered membrane system studied in this thesis consists of three different regions: the electrical double layers at the

gold electrodes, the bulk electrolyte reservoir, and the tethered membrane.

The electrical double layers are composed of a bound region of ions, and a diffusive region, which can be modeled using an overall capacitance C_{tdl} on one side of bioelectronic interface, and C_{bdl} on the other side. Furthermore, the bulk electrolyte reservoir can be modeled by a pure ohmic resistance R_e. Moreover, since a tethered membrane can be regarded as a uniformly polarized structure, it could be modeled by another capacitance C_m. Additionally, the so-called "electroporation" phenomenon, which states the effect that numerous pores can form on surface of membrane when an excitation potential $V_s(t)$ is presented, can be modeled by a membrane conductance G_m.

The macroscopic model is based on the equivalent circuit model stated above, however, a fractional order operator must be included to account for the diffusion limited processes present at the bioelectronic interface of the tethered membrane. A diffusion limited process refers to the effect that membrane molecules at the interface will diffuse and contact the bioelectronic interface, thus to trigger a fast reaction of charge transfer of bio-molecules. An overview of the fractional order macroscopic model is presented in Fig. 3.7.

3.6.1 Fractional Order Macroscopic Model and Parameter Estimation

In this subsection, a fractional order macroscopic model of the tethered archaebacterial membrane is provided. This model estimates the membrane conductance G_m and capacitance C_m, from the experimentally measured current response of the tethered membrane. The membrane conductance G_m is dependent on the diffusion dynamics of lipids, line tension γ, and the surface tension σ; while the membrane capacitance C_m is dependent on the thickness of the membrane h_m.

How do we obtain the necessary parameters to calculate membrane conductance and inductance? Recall that the diffusion dynamics, line tension, surface tension, and membrane thickness can be computed from the CGMD simulation results. Fractional order operators are utilized in the macroscopic model, as the gold surface (the bioelectronic interface) of the tethered membrane may contain diffusion-limited charge transfer, quasi-reversible charge transfer, and ionic adsorption dynamics. These double-layer charging effects can be modeled using fractional order operators [8].

The tethered archaebacterial membrane is composed of three distinct regions: the bioelectronic interface at the gold electrodes, the tethered

membrane, and the bulk electrolyte solution. The membrane is assumed to be uniformly polarizable and contain aqueous pores as a result of random thermal fluctuations. This allows the tethered membrane to be modeled by a capacitance C_m in parallel with the tethered membrane conductance G_m [23, 26, 27]. The membrane conductance is time dependent as a result of variations in the concentration of conducting aqueous pores in the tethered archaebacterial membrane. The bulk electrolyte solution is assumed to be purely ohmic with a resistance R_e.

Due to the diffusion limited process, there exists an electrical double layer [30] at the bioelectronic interface, which can be modeled using a capacitor if diffusion-limited charge transfer, quasireversible charge transfer, and ionic adsorption dynamics are not present. If these double-layer charging effects are present then the bioelectronic interface can be modeled using a constant-phase-element composed of a capacitance and the fractional order operator p. If $p < 1$ then a diffusion-limited process is present, and if $p = 1$ then a diffusion-limited process is not present. An excitation potential V_s is applied across the two electrodes of the tethered membrane and the current response I is measured. The fractional order macroscopic model of the tethered membrane is given by (Fig. 3.7):

$$\begin{aligned}
\frac{dV_m}{dt} &= -(\frac{1}{C_m R_e} + \frac{G_m}{C_m})V_m - \frac{1}{C_m R_e}V_{dl} + \frac{1}{C_m R_e}V_s, \\
\frac{d^p V_{dl}}{dt^p} &= -\frac{1}{C_{dl} R_e}V_m - \frac{1}{C_{dl} R_e}V_{dl} + \frac{1}{C_{dl} R_e}V_s, \qquad (3.27)
\end{aligned}$$

$$I(t) = \frac{1}{R_e}\big(V_s - V_m - V_{dl}\big), \qquad (3.28)$$

where C_{dl} is the total capacitance of C_{tdl} and C_{bdl} in series with p in Eq. 3.27 the fractional order operator, V_m the transmembrane potential, and V_{dl} the double-layer charging potential.

The tethered membrane conductance G_m is modeled using asymptotic approximations to the Smoluchowski-Einstein equation [27]. The equations governing the dynamics of G_m are provided as follows:

$$
\begin{aligned}
G_m &= \sum_{i=1}^{\lfloor N(t) \rfloor} G_p(r_i), \qquad (3.29)\\
\frac{dr_i}{dt} &= -\frac{D}{k_B T}\frac{\partial W}{\partial r_i} \quad \text{for} \quad r_i \in \{1, 2, \ldots, \lfloor N(t) \rfloor\},\\
\frac{dN}{dt} &= \alpha e^{(\frac{V_m}{V_{ep}})^2}\big(1 - \frac{N}{N_o} e^{-q(\frac{V_m}{V_{ep}})^2}\big),\\
W(r, V_m) &= 2\pi\gamma r - \pi\sigma r^2 + (\frac{C}{r})^4 + W_{\text{es}}(r, V_m) - W_{\text{m}}
\end{aligned}
$$

In Eq. 3.29, α is the pore creation rate coefficient, V_{ep} is the characteristic voltage of electroporation (i.e. the voltage at which the effects of electroporation are non-negligible), N_o is the equilibrium pore density at $V_m = 0$, and $q = (r_m/r_*)^2$ is the squared ratio of the minimum energy radius r_m at $V_m = 0$ with r_* the minimum energy radius of hydrophilic pores [29, 41, 48, 61]. W is the hydrophobic aqueous pore energy and consists of four energy terms: the pore edge energy γ, the membrane surface tension σ, the electrostatic interaction between lipid heads, and the transmembrane potential energy contribution W_{es}. The parameters G_p and W_{es} are provided in [27].

For a membrane containing negligible defects the parameters C_m, C_{dl}, p, R_e are constant with G_m dependent on the transmembrane potential.

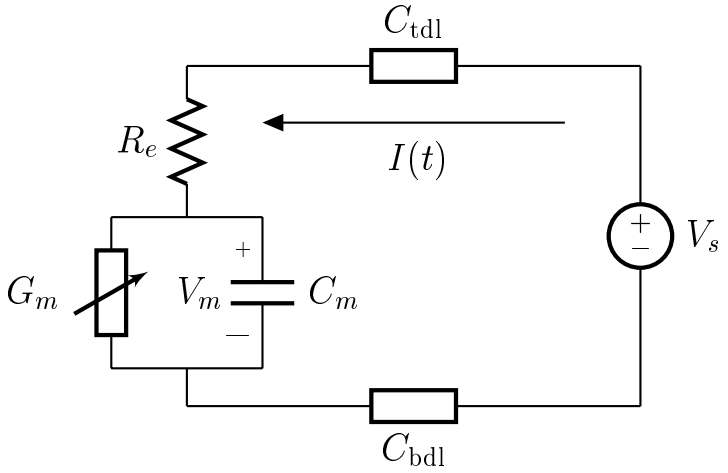

Figure 3.7: Fractional order macroscopic model of the tethered archaebacterial membrane. The circuit parameters are defined in the Tethered Archaebacterial Membrane section.

For a transmembrane potential below 50 mV, G_m can be regarded as constant and represents the equilibrium number of aqueous pores in the tethered membrane. To estimate the equilibrium conductance and parameters in Eq. 3.27, impedance measurements from the tethered membrane can be used. For a sinusoidal drive potential $V_s(t) = V_o \sin(2\pi f t)$ with frequency f and magnitude V_o below 50 mV, the impedance, denoted by $Z(f)$ of the tethered membrane is given by:

$$Z(f) = R_e + \frac{1}{G_m + j2\pi f C_m} + \frac{1}{(j2\pi f)^p C_{dl}}. \tag{3.30}$$

In Eq. 3.30, j denotes the imaginary part of complex number $\sqrt{-1}$. Given the difference of the experimentally measured impedance and the numerically predicted impedance from Eq. 3.30, the parameters in Eq. 3.27 can be evaluated by using a least-square estimator. For instance, the constrained optimization function "fmincon" in Matlab is able to estimate the parameters. For the case of 0% cholesterol, by using the experimental measurements of impedance, fmincon gives membrane capacitance $C_m = 34.4nF$, membrane conductance $G_m = 0.48\mu S$, the fractional order $p = 0.95$. As shown in Fig 3.8, the parameters obtained from least-square estimator are in excellent agreement with experimental data.

For transmembrane potentials above 50 mV, the membrane conductance is dependent on parameters such as the line tension and surface tension of the membrane. To model the dynamics of G_m and the double-layer charging effects of the tethered membrane, Eq. 3.27 is required to be coupled with the Smoluchowski-Einstein equation 3.29, which governs the current response I of the tethered membrane given a drive potential V_s.

3.6.2 Experimental Results Utilizing the Macroscopic Model

In this subsection, experimental measurements from the tethered archaebacterial membrane are provided, such that the CGMD simulation results can be validated. By using the fractional order macroscopic model, the experimental measurements can be used to calculate the membrane conductance G_m and membrane capacitance C_m. G_m is dependent on the diffusion coefficient D, surface tension σ, line tension γ. C_m is dependent on the membrane thickness h_m and area A_m. Prior to all experimental measurements, the membrane integrity and static parameters in the fractional order macroscopic model are evaluated using impedance measurements. The parameters are summarized in Table 3.3. The fractional order operator p is

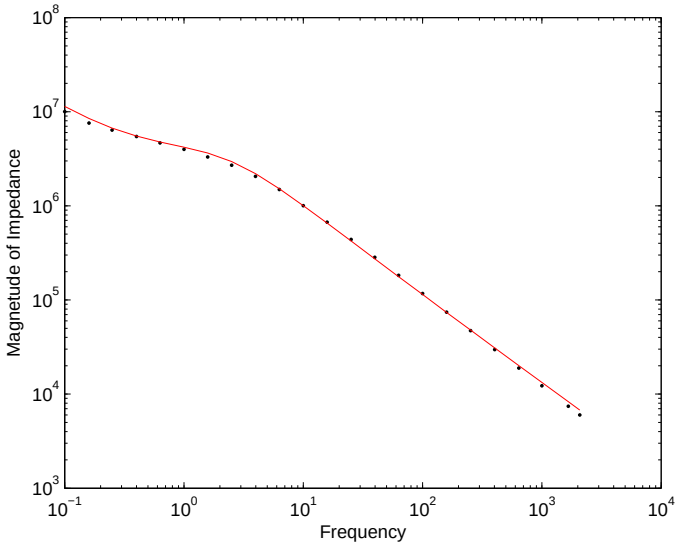

Figure 3.8: The data fitting of estimated parameters in Eq 3.27 (red), which are obtained from experimental impedance measurements (black dot) with V_m below 50mV, for the membrane with 0% cholesterol.

in the range of 0.95 to 0.98, this confirms that a diffusion-limited process is present at the bioelectronic gold interface of the tethered archaebacterial membrane. The associated capacitance C_{dl} is in the range of 120 nF to 180 nF. The membrane capacitance C_m, conductance G_m, and characteristic voltage of electroporation V_{ep} are provided in Table 1.

Fig. 3.9 provides the experimentally measured and numerically predicted current response of the tethered archaebacterial membrane for different mol % concentrations of cholesterol. The computed current is in excellent agreement with the experimentally measured current response of the tethered archaebacterial membrane. This confirms the experimental measurements and macroscopic model to estimate important biological parameters, which can be used to validate results from the CGMD model.

Electroporation refers to a biophysical method that uses an electrical pulse to create temporary pores in cell membranes. The characteristic voltage of electroporation, denoted by V_{ep}, is the threshold voltage under which the first pores appear on the membrane surface. An interesting question is, how does the concentration of cholesterol affect V_{ep} in the tethered archaebacterial membrane? From Table 3.3 we see that as the

concentration of cholesterol increases there is an increase in V_{ep}. This is in agreement with the results that typically seen for membranes containing POPC [10], DPPC [25], DphPC [68], phosphatidylcholine, phosphatidylserine and phosphatidyl-glycerol lipid bilayers [38], and egg yolk phosphatidylcholine bilayer [40], in which an increase in cholesterol increases the stability of the membrane (i.e. increases V_{ep} and decreases G_m).

Furthermore, what effects cholesterol has on the equilibrium membrane conductance G_m? For 0% to 30% cholesterol concentrations the membrane conductance decreases for increasing % of cholesterol. At an atomistic level, one possible explanation for the decrease in G_m is the packing of the hydrocarbon chains in the DphPC and GDPE lipids. For DphPC membranes the phytanyl tails form a tightly packed network with neighbouring hydrocarbon chains being interdigitated [33, 58, 59]. The addition of a low percentage of cholesterol (below 30 %) causes the DphPC and GDPE molecules to condense the phospholipid network resulting in a decrease in G_m. Interestingly, as the concentration of cholesterol increases above 30%, there is an increase in G_m. This suggests that large concentrations of cholesterol in the archaebacterial membrane cause the disentanglement of the phytanyl chains in the DphPC and GDPE lipids which introduce membrane defects into the membrane [68].

Table 3.3: Macroscopic Model Parameters for Archaebacterial Membrane

% Cholesterol	p	C_m	G_m	V_{ep}
0	0.95	34.4 nF	0.48μS	270 mV
10	0.95	32.4 nF	0.26μS	290 mV
20	0.95	31.4 nF	0.25μS	300 mV
30	0.95	31 nF	0.24μS	330 mV
40	0.95-0.98	35 nF	1.00μS	345 mV
50	0.95-0.98	41 nF	1.11μS	350 mV

G_m is the equilibrium membrane conductance, C_m the membrane capacitance, V_{ep} the characteristic voltage of electroporation, and p the fractional order parameter.

3.7 Summary

In order to gain insights into the diffusion dynamics and biomechanics of archaebacterial membranes containing different concentrations of cholesterol,

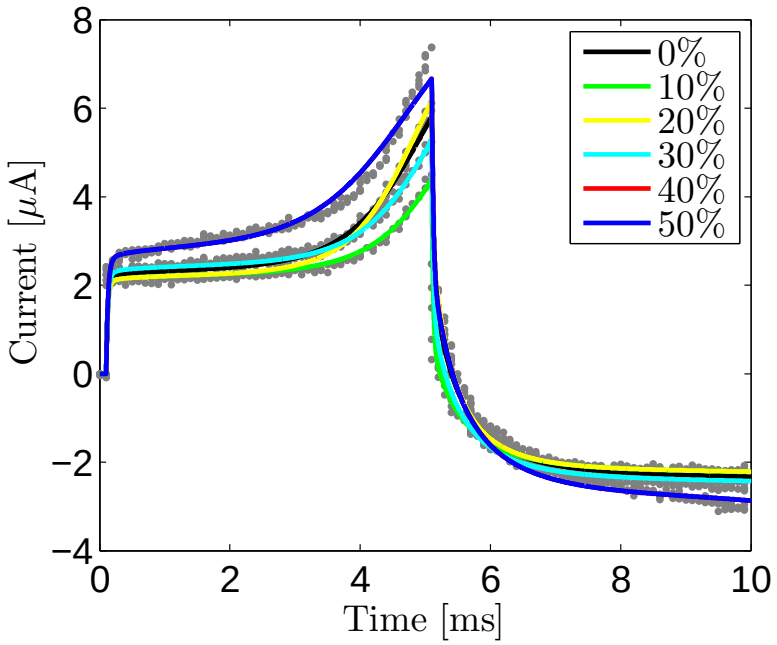

Figure 3.9: Experimentally measured (gray dots) and numerically predicted current response for tethered membranes containing cholesterol. The parameters for the numerical predictions are given in Table 3.3. The excitation V_s is given by a linearly increasing voltage with rate of 100 V/s for 5 ms, then a linearly decreasing voltage with a rate of -100 V/s for 5 ms.

a CGMD model based on the MARTINI force field is constructed for a synthetic archaebacterial membrane, which is composed of 70% DphPC and 30% GDPE lipids. By using the CGMD model and experimental measurements, several key insights are provided.

The diffusion dynamics of cell membrane lipids is investigated using trajectory results of CGMD simulation. It is shown that the transition time between the subdiffusion and Fickian diffusion regimes for lipids is not dependent on the concentration of cholesterol in the membrane. The concentration of cholesterol only affects the diffusion coefficient of lipids in the Fickian diffusion regime–for increasing cholesterol content, the lipid diffusion coefficients decrease.

To ensure that the bioelectronic interface do not effect the membrane response, we computed the position dependent density of water at the bioelectronic interface. It is illustrated that the bioelectronic interface does not

contribute to the dynamics and biomechanics of the archaebacterial membrane. Additionally, by using approximations to the Yvan-Born-Green integral equation, the analytical solution of Percus-Yevick solution is matched with water density profile from CGMD simulation. It is shown that harsh repulsive forces play a negligible role in the long range dynamics of the position dependent density profile of water at the bioelectronic interface.

Biomechanic properties of membrane lipids with cholesterol are checked based on CGMD simulation results. For concentrations of cholesterol below 30% the membrane surface tension increases with increasing cholesterol content, however beyond 30% the surface tension decreases. For increasing concentrations of cholesterol from 0% to 50%, the line tension of the membrane increases. These results are validated using experimental measurements from tethered archaebacterial membranes, when a fractional order macroscopic model is used to link the simulation results with experimental measurements.

Chapter 4

Summary and Future Work

A study of cholesterol in tethered membrane system using coarse-grained molecular dynamics simulations was presented in this thesis. By discussing modified properties of synthetic archaebacterial membrane with different concentrations of cholesterol, this research work presented a balance of accuracy and efficiency of CGMD simulations, along with various mathematical techniques that are used to investigate bio-systems at atomistic level.

Chapter 1 gave a brief description of biosensor, which motivates the research on membrane system tethered onto a bioelectronic interface. Since this study is based on simulations to predict membrane properties, five levels of modeling abstraction in bio-system modeling were explained. Among these abstractions, coarse-grained molecular dynamics simulation was chosen for this work, due to its fair accuracy and high efficiency of computation.

Chapter 2 presented an introduction to concepts and theories involved in molecular dynamics. The MD simulation engine GROMACS was introduced, along with an explanation on the MARTINI coarse grained force field. Then a four-step scheme of CGMD simulation using GROMACS was discussed in details, which includes:

- Setting up specific formatted files and programs in GROMACS with proper configurations for the initial state of simulated system.
- Minimizing the potential energy for the states whenever the system files are changed to ensure the simulation starts at a state that is close enough to equilibrium.
- Executing the production run simulation after proper energy minimization as long as the xxx.mdp file is configured to include parameters for a desired ensemble.
- Using the recorded coordinate and energy information as a function of time to gain insights into characteristics of the bio-system.

Chapter 3 presented the core research work in this thesis. A CGMD model based on MARTINI force field was constructed to study effects of cholesterol on a synthetic tethered archaebacterial membrane, which is composed

of 70% DphPC and 30% GDPE lipids. The diffusion dynamics of lipids, thickness of membrane, surface tension, and line tension of membrane were studied corresponding to different concentrations of cholesterol added to the membrane. By using the CGMD model and experimental measurements, several key insights were provided.

In order to ensure that the bioelectronic surface does not affect membrane response, position dependent water density profile at the two bioelectronic interface was investigated. The analytical solution of Percus-Yevick equation obtained as an approximation from Yvan-Born-Green integral equation was discussed. It was shown that at about 4 nm from the interface, the water density profile doesn't vary much and harsh short-range interactions in Lennard-Jones potential do not affect water density profile.

Furthermore, it was observed that the concentrations of cholesterol do not affect the transition time between the sub-diffusion region and Fickian diffusion, which are predicted by MCT theory and can be computed from Volterra integro-differential equation. The concentration of cholesterol only affects the diffusion coefficient of lipids in the Fickian diffusion regime - for increasing cholesterol levels, the lipid diffusion coefficients decrease.

Finally, experimental measurements were used to validate the simulation results using a fractional order macroscopic model. It was confirmed that, as the concentrations of cholesterol increase from 0% to 50% - the diffusion coefficients of tethered archaebacterial membrane decrease, the membrane thickness and line tension increases, while surface tension increases up to 30% cholesterol then decreases.

Potential future work includes obtaining numerical solution of Volterra integral-differential equation up to femto-second scale, and using resonance energy transfer [12] to obtain experimental data for the diffusion coefficient of membrane components to further validate the simulation results.

Bibliography

[1] BJ Alder and TEf Wainwright. Phase transition for a hard sphere system. *The Journal of Chemical Physics*, 27(5):1208, 1957.

[2] PFF Almeida and WLC Vaz. Lateral diffusion in membranes. *Handbook of biological physics*, 1:305–357, 1995.

[3] A. Archer and R. Evans. Relationship between local molecular field theory and density functional theory for non-uniform liquids. *The Journal of chemical physics*, 138(1):014502, 2013.

[4] T. Baba, H. Minamikawa, M. Hato, and T. Handa. Hydration and molecular motions in synthetic phytanyl-chained glycolipid vesicle membranes. *Biophysical journal*, 81(6):3377–3386, 2001.

[5] D. Bennett, J. MacCallum, and P. Tieleman. Thermodynamic analysis of the effect of cholesterol on dipalmitoylphosphatidylcholine lipid membranes. *Journal of the American Chemical Society*, 131(5):1972–1978, 2009.

[6] Herman JC Berendsen, David van der Spoel, and Rudi van Drunen. Gromacs: A message-passing parallel molecular dynamics implementation. *Computer Physics Communications*, 91(1):43–56, 1995.

[7] M. Berkowitz. Detailed molecular dynamics simulations of model biological membranes containing cholesterol. *Biochimica et Biophysica Acta (BBA)-Biomembranes*, 1788(1):86–96, 2009.

[8] P. Bressloff and J. Newby. Stochastic models of intracellular transport. *Review Modern Physics*, 85:135–196, 2013.

[9] G. Bussi, D. Donadio, and M. Parrinello. Canonical sampling through velocity rescaling. *J. Chem. Phys.*, 126:014101, 2007.

[10] M. Casciola, D. Bonhenry, M. Liberti, F. Apollonio, and M. Tarek. A molecular dynamic study of cholesterol rich lipid membranes: comparison of electroporation protocols. *Bioelectrochemistry*, 100:11–17, 2014.

[11] S. Chong, M. Aichele, H. Meyer, M. Fuchs, and journal= Baschnagel, J. Structural and conformational dynamics of supercooled polymer melts: Insights from first-principles theory and simulations.

[12] S. Chong and M. Fuchs. Mode-coupling theory for structural and conformational dynamics of polymer melts. *Physical review letters*, 88(18):185702, 2002.

[13] Jr Leland C Clark. Electrochemical device for chemical analysis, November 17 1959. US Patent 2,913,386.

[14] Charles G Cranfield, Bruce A Cornell, Stephan L Grage, Paul Duckworth, Sonia Carne, Anne S Ulrich, and Boris Martinac. Transient potential gradients and impedance measures of tethered bilayer lipid membranes: pore-forming peptide insertion and the effect of electroporation. *Biophysical journal*, 106(1):182–189, 2014.

[15] M. Daily, B. Olsen, P. Schlesinger, D. Ory, and N. Baker. Improved coarse-grained modeling of cholesterol-containing lipid bilayers. *Journal of chemical theory and computation*, 10(5):2137–2150, 2014.

[16] Nathalie Fa, Sébastien Ronkart, André Schanck, Magali Deleu, Anthoula Gaigneaux, Erik Goormaghtigh, and M-P Mingeot-Leclercq. Effect of the antibiotic azithromycin on thermotropic behavior of dopc or dppc bilayers. *Chemistry and physics of lipids*, 144(1):108–116, 2006.

[17] L. Fernndez, G. Marshall, F. Sagus, and R. Reigada. Structural and kinetic molecular dynamics study of electroporation in cholesterol-containing bilayers. *The Journal of Physical Chemistry B*, 114(20):6855–6865, 2010.

[18] A. Filippov, G. Ordd, and G. Lindblom. Domain formation in model membranes studied by Pulsed-Field Gradient-NMR: The role of lipid Polyunsaturation. *Biophysical Journal*, 93(9):3182 – 3190, 2007.

[19] E. Flenner, J. Das, M. Rheinstädter, and I. Kosztin. Subdiffusion and lateral diffusion coefficient of lipid atoms and molecules in phospholipid bilayers. *Physical Review E*, 79(1):011907, 2009.

[20] Inga Gustafson. Phospholipid membranes in biosensor applications: Stability, activity and kinetics of reconstituted proteins and glycolipids in supported membranes. 2004.

[21] J. Hansen and I. McDonald. *Theory of simple liquids*. Elsevier, 1990.

[22] W Keith Hastings. Monte carlo sampling methods using markov chains and their applications. *Biometrika*, 57(1):97–109, 1970.

[23] F. Heinrich, T. Ng, D. Vanderah, P. Shekhar, M. Mihailescu, H. Nanda, and M. Losche. A new lipid anchor for sparsely tethered bilayer lipid membranes. *Langmuir*, 25(7):4219–4229, 2009.

[24] B. Hess, C. Kutzner, D. Spoel, and E. Lindahl. Gromacs 4: algorithms for highly efficient, load-balanced, and scalable molecular simulation. *J. Comput. Chem*, 4:435–447, 2008.

[25] C. Hofsäß, E. Lindahl, and O. Edholm. Molecular dynamics simulations of phospholipid bilayers with cholesterol. *Biophysical journal*, 84(4):2192–2206, 2003.

[26] W. Hoiles, V. Krishnamurthy, and B. Cornell. Modelling the bioelectronic interface in engineered tethered membranes: from biosensing to electroporation. *IEEE Transactions on Biomedical Circuits and Systems*, PP(99):1–13, 2014.

[27] W. Hoiles, V. Krishnamurthy, C. Cranfield, and B. Cornell. An engineered membrane to measure electroporation: Effect of tethers and bioelectronic interface. *Biophysical journal*, 107(6):1339–1351, 2014.

[28] Wm G Hoover. Molecular dynamics. In *Molecular Dynamics*, volume 258, 1986.

[29] Q. Hu and R. Joshi. Transmembrane voltage analyses in spheroidal cells in response to an intense ultrashort electrical pulse. *Physical Review E*, 79:011901, 2009.

[30] Z. Hughes and T. Walsh. Structure of the electrical double layer at aqueous gold and silver interfaces for saline solutions. *Journal of Colloid and Interface Science*, 436(0):99 – 110, 2014.

[31] William Humphrey, Andrew Dalke, and Klaus Schulten. Vmd: visual molecular dynamics. *Journal of molecular graphics*, 14(1):33–38, 1996.

[32] W. Hung, M. Lee, F. Chen, and H. Huang. The condensing effect of cholesterol in lipid bilayers. *Biophysical Journal*, 92(11):3960–3967, 2007.

[33] T. Husslein, D. Newns, P. Pattnaik, Q. Zhong, P. Moore, and M. Klein. Constant pressure and temperature molecular-dynamics simulation of the hydrated diphytanolphosphatidylcholine lipid bilayer. *The Journal of chemical physics*, 109(7):2826–2832, 1998.

[34] E. Ikonen. Cellular cholesterol trafficking and compartmentalization. *Nature Reviews Molecular Cell Biology*, 9(2):125–138, 2008.

[35] F. Jiang, Y. Bouret, and J. Kindt. Molecular dynamics simulations of the lipid bilayer edge. *Biophys. J.*, 87:182–192, 2004.

[36] Y. Jiang and J. Kindt. Simulations of edge behaviour in a mixed bilayer: Flctuation analysis. *J. Chem. Phys.*, 126:045105–9, 2007.

[37] J. Joannis, F. Jiang, and J. Kindt. Coarse-grained model simulations of mixed-lipid systems: Composition and line tension of a stabilized bilayer edge. *Langmuir*, 22:998–1005, 2006.

[38] S. Kakorin, U. Brinkmann, and E. Neumann. Cholesterol reduces membrane electroporation and electric deformation of small bilayer vesicles. *Biophysical chemistry*, 117(2):155–171, 2005.

[39] Barbara Kirchner, Philipp J di Dio, and Jürg Hutter. Real-world predictions from ab initio molecular dynamics simulations. In *Multiscale Molecular Methods in Applied Chemistry*, pages 109–153. Springer, 2012.

[40] S. Koronkiewicz and S. Kalinowski. Influence of cholesterol on electroporation of bilayer lipid membranes: chronopotentiometric studies. *Biochimica et Biophysica Acta (BBA)-Biomembranes*, 1661(2):196–203, 2004.

[41] W. Krassowska and P. Filev. Modeling electroporation in a single cell. *Biophysical Journal*, 92(2):404 – 417, 2007.

[42] Raphael D Levine. *Molecular reaction dynamics*. Cambridge University Press, 2005.

[43] C. Liu and R. Faller. Conformational, dynamical. and tensional study of tethered bilayer lipid membranes in coarse-grained molecular simulations. *Langmuir*, 28:15907–15915, 2012.

[44] Harvey F Lodish, Arnold Berk, S Lawrence Zipursky, Paul Matsudaira, David Baltimore, James Darnell, et al. *Molecular cell biology*, volume 4. Citeseer, 2000.

[45] S. Marrink, H. Risselada, D. Yefimov, D. Tieleman, and A. Vries. The martini force field: Coarse grained model for biomolecular simulations. *J. Phys.Chem.B*, 111:7812–7824, 2007.

[46] S. Marrink and P. Tieleman. Perspective on the MARTINI model. *Chem. Soc. Rev.*, 42:6801–6822, 2013.

[47] Siewert J Marrink, H Jelger Risselada, Serge Yefimov, D Peter Tieleman, and Alex H De Vries. The martini force field: coarse grained model for biomolecular simulations. *The Journal of Physical Chemistry B*, 111(27):7812–7824, 2007.

[48] S. Movahed and D. Li. A theoretical study of single-cell electroporation in a microchannel. *Journal of Membrane Biology*, 246:151–160, 2013.

[49] H. Ohvo-Rekilä, B. Ramstedt, P. Leppimäki, and P. Slotte. Cholesterol interactions with phospholipids in membranes. *Progress in lipid research*, 41(1):66–97, 2002.

[50] I Palchetti and M Mascini. Biosensor technology: a brief history. In *Sensors and Microsystems*, pages 15–23. Springer, 2010.

[51] JJ Pancrazio, JP Whelan, DA Borkholder, W Ma, and DA Stenger. Development and application of cell-based biosensors. *Annals of biomedical engineering*, 27(6):697–711, 1999.

[52] R. Reigada. Electroporation of heterogeneous lipid membranes. *Biochimica et Biophysica Acta (BBA)-Biomembranes*, 1838(3):814–821, 2014.

[53] WR Reinmuth. Theory of diffusion limited charge-transfer processes in electroanalytical techniques. *Analytical Chemistry*, 34(11):1446–1454, 1962.

[54] Mantripragada B Sankaram and Thomas E Thompson. Modulation of phospholipid acyl chain order by cholesterol. a solid-state deuterium nuclear magnetic resonance study. *Biochemistry*, 29(47):10676–10684, 1990.

[55] Mantripragada B Sankaram and Thomas E Thompson. Cholesterol-induced fluid-phase immiscibility in membranes. *Proceedings of the National Academy of Sciences*, 88(19):8686–8690, 1991.

[56] H. Scheidt, D. Huster, and K. Gawrisch. Diffusion of cholesterol and its precursors in lipid membranes studied by 1h pulsed field gradient magic angle spinning NMR. *Biophysical Journal*, 89(4):2504 – 2512, 2005.

[57] Y. Shen, P. Saboe, I. Sines, M. Erbakan, and M. Kumar. Biomimetic membranes: a review. *Journal of Membrane Science*, 454:359–381, 2014.

[58] K. Shinoda, W. Shinoda, T. Baba, and M. Mikami. Comparative molecular dynamics study of ether-and ester-linked phospholipid bilayers. *The Journal of chemical physics*, 121(19):9648–9654, 2004.

[59] W. Shinoda, M. Mikami, T. Baba, and M. Hato. Molecular dynamics study on the effect of chain branching on the physical properties of lipid bilayers: structural stability. *The Journal of Physical Chemistry B*, 107(50):14030–14035, 2003.

[60] A Singer, D Gillespie, J Norbury, and RS Eisenberg. Singular perturbation analysis of the steady-state poisson–nernst–planck system: Applications to ion channels. *European journal of applied mathematics*, 19(05):541–560, 2008.

[61] K. Smith, J. Neu, and W. Krassowska. Model of creation and evolution of stable electropores for DNA delivery. *Biophysical Journal*, 86(5):2813 – 2826, 2004.

[62] A. Smondyrev and M. Berkowitz. Structure of dipalmitoylphosphatidylcholine/cholesterol bilayer at low and high cholesterol concentrations: Molecular dynamics simulation. *Biophysical Journal*, 77(4):2075 – 2089, 1999.

[63] P. Stroeve and I. Miller. Lateral diffusion of cholesterol in monolayers. *Biochimica et Biophysica Acta (BBA) - Biomembranes*, 401(2):157 – 167, 1975.

[64] Seyed R Tabaei, Joshua A Jackman, Seong-Oh Kim, Bo Liedberg, Wolfgang Knoll, Atul N Parikh, and Nam-Joon Cho. Formation of cholesterol-rich supported membranes using solvent-assisted lipid self-assembly. *Langmuir*, 30(44):13345–13352, 2014.

[65] Leung Tsang, Jin Au Kong, Kung-Hau Ding, and Chi On Ao. *Front-matter and Index*. Wiley Online Library, 2001.

[66] K. Tu, M. Klein, and D. Tobias. Constant-pressure molecular dynamics investigation of cholesterol effects in a dipalmitoylphosphatidylcholine bilayer. *Biophysical Journal*, 75(5):2147 – 2156, 1998.

[67] David Turnbull and Morrel H Cohen. On the free-volume model of the liquid-glass transition. *The journal of chemical physics*, 52(6):3038–3041, 1970.

[68] I. Uitert, S. Gac, and A. Berg. The influence of different membrane components on the electrical stability of bilayer lipid membranes. *Biochimica et Biophysica Acta (BBA)-Biomembranes*, 1798(1):21–31, 2010.

[69] David van der Spoel, Erik Lindahl, Berk Hess, AR Van Buuren, E Apol, PJ Meulenhoff, DP Tieleman, ALTM Sijbers, KA Feenstra, Rudi van Drunen, et al. Gromacs user manual version 3.3. 2008.

[70] E. Waisman, D. Henderson, and J. Lebowitz. Solution of the mean spherical approximation for the density profile of a hard-sphere fluid near a wall. *Molecular Physics*, 32(5):1373–1381, 1976.

[71] J. Weeks, K. Katsov, and K. Vollmayr. Roles of repulsive and attractive forces in determining the structure of nonuniform liquids: Generalized mean field theory. *Physical review letters*, 81(20):4400, 1998.

[72] J. Weeks, K. Vollmayr, and K. Katsov. Intermolecular forces and the structure of uniform and nonuniform fluids. *Physica A: Statistical Mechanics and its Applications*, 244(1):461–475, 1997.

[73] M. Wertheim. Exact solution of the percus-yevick integral equation for hard spheres. *Physical Review Letters*, 10(8):321–323, 1963.

[74] J. Wohlert, W. Otter, O. Edholm, and W. Briels. Free energy of a transmembrane pore calculated from atomistic molecular dynamics simulations. *The Journal of chemical physics*, 124(15):154905, 2006.

[75] D. Zhelev and D. Needham. Tension-stabilized pores in giant vesicles: determination of pore size and pore line tension. *Biochim. Biophys. Acta*, 1147:89–104, 1993.

[76] S. Zhou and A. Jamnik. Structure of inhomogeneous lennard-jones fluid near the critical region and close to the vapor-liquid coexistence curve: Monte Carlo and density-functional theory studies. *Physical Review E*, 73(1):011202, 2006.

Appendix A

Matlab Code to Calculate the Percus Yevick Pair Distribution Function for Spherical Particles

Matlab Code

```
% This code is originally contributed by K.H. Ding (2008) and edited by
% Yan Duan (2015) at UBC to calculate the Percus Yevick pair distribution
% function for spherical particles

clc;
clear all;
% Initialization of parameters from Eq. (3.5)- Eq. (3.11)
n0=1;
% Set the diameter of spherical particles, units in nm
dia=0.99;
s=1;
tau=9;
tauc=(2-sqrt(2))/6;
xic=(3*sqrt(2)-4)/2;
rm=20;
nk=1000;
dk=pi/(rm*dia);
dr=rm*dia/(nk+1);
hk=zeros(2*nk+2,1);
vol=pi*dia^3/6;
```

```
% Fractional Volume
fv=n0*vol;
f=fv;
% calculate the parameters of c(r) in Eq. (3.9)
denom=1-f;
nu=tau+f/denom;
epsilon=f*(1+f/2)/(3*denom^2);
lamd=6*(nu-sqrt(nu^2-epsilon))/f;
mu=lamd*f*denom;
if mu > 1+2*f
   break;
end

alpha=f/denom;
beta=1-lamd*f+3*alpha;
gamma=3-lamd*denom;
% Open the file to write c(r)
fpk=fopen('pysf.dat','w+');

pk=0;
pp1=alpha*(4-lamd+3*alpha)+1;
pp2=0;
pyhk=(1/(pp1^2+pp2^2)-1)/n0;
pysf=1+pyhk*n0;
fprintf(fpk,'%6u %14.9f \n',pk,pysf);

% calculate h(r) in terms of c(r)
for ik=1:nk
   pk=ik*dk;
   x=pk*dia/2;
   snx=sin(x);
   csx=cos(x);
   psix=snx/x;
   phix=3*(snx-x*csx)/(x^3);
   pp1=alpha*(beta*phix+gamma*psix)+csx;
   pp2=alpha*x*phix+snx;
   pyhk=(1/(pp1^2+pp2^2)-1)/n0;
   pysf=1+pyhk*n0;
   fprintf(fpk,'%6u %14.9f \n',pk,pysf);
   hk(ik+1)=pk*pyhk;
```

```
61 end
62 fclose(fpk);
63
64 % fourier transform
65 hw=-2*fft(hk);
66 hr=imag(hw(2:nk+1));
67
68 fpr=fopen('pypdf.dat','w+');
69 % reverse fourier transform and write h(r)
70 for ir=1:nk
71   r=ir*dr/dia;
72   if r >= 1
73     g=1+hr(ir)/(rm*4*pi*r*dia^2);
74     fprintf(fpr,'%14.9f %14.9f \n',r,g);
75   end
76 end
77 fclose(fpr);
78 % plot pair distribution function
79 load pypdf.dat -ascii;
80 load pysf.dat -ascii;
81 % scale the distribution plot
82 for i=[1:length(pypdf(:,2))]
83     if -pypdf(i,1)+41.55>39 && -pypdf(i,1)+41.55<41
84         pypdf(i,2)=pypdf(i,2)/1.5+0.31;
85     end
86 end
87 % Plot the analytical solution of Percus-Yevick
     equation
88 figure(1);
89 x = 19.7*ones(1,2300);
90 y = 1:2300;
91 plot(x,y,'linewidth',2);
92 hold on;
93 x_analytical=(-pypdf(8:800,1)+41.55)*0.4755;
94 y_analytical=(pypdf(8:800,2)-0.45)*1800;
95 plot(x_analytical,y_analytical,'r','linewidth',2);
96 axis([12,20,0.0,2700]);
97
98 xlabel('r (nm) ');
99 ylabel('\rho(r) ');
```

```
100 hold on;
101 % Import the CGMD simulation results
102 A=importdata('density.xvg');
103
104 x_CGMD=A(:,1);
105 y_CGMD=A(:,2);
106 plot(A(:,1),A(:,2),'--','linewidth',2);
107
108 legend('Analytical','CGMD');
109 fillPage(gcf, 'papersize', [5 3],'margins',[0 0 0 0]);
110 xlabel('position z[nm]');
111 ylabel('water density');
112 print -deps epsFig
```